Gastroenterology 2025;■:1–17

KRASG12D Cells Override Homeostatic Cell Elimination Mechanisms in Adult Pancreas Via Wnt5a and Cell Dormancy

Beatriz Salvador-Barbero,[1] Markella Alatsatianos,[1] Jennifer P. Morton,[2,3] Owen J. Sansom,[2,3] and Catherine Hogan[1]

[1]European Cancer Stem Cell Research Institute, School of Biosciences, Cardiff University, Cardiff, UK; [2]Cancer Research UK Scotland Institute, Glasgow, UK; and [3]School of Cancer Sciences, University of Glasgow, Glasgow, UK

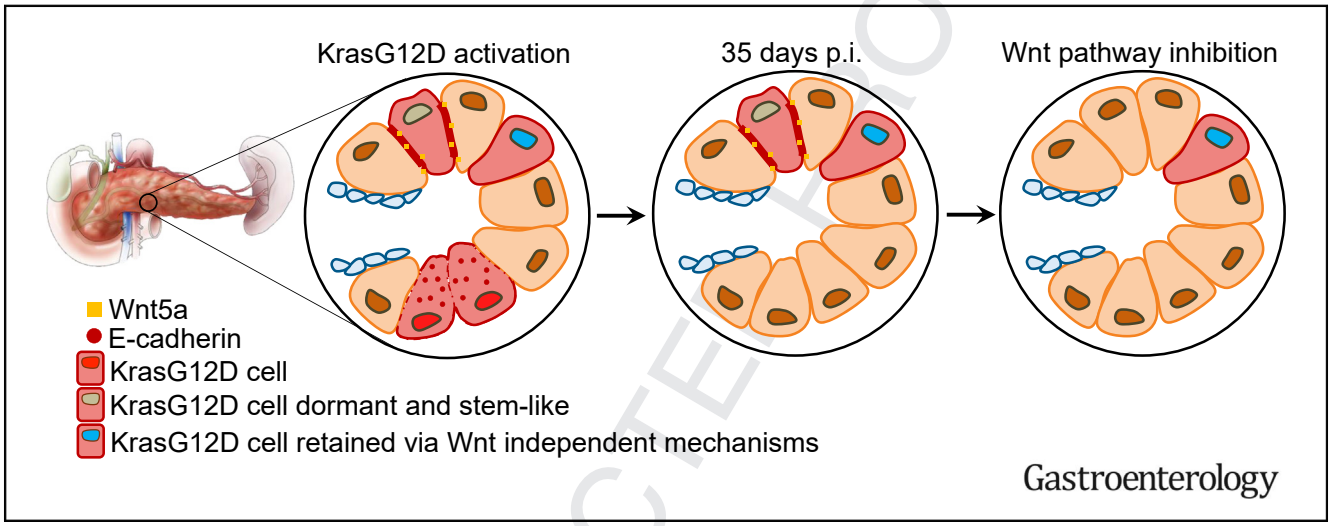

BACKGROUND & AIMS: The adult pancreas protects against cancer by actively expelling genetically mutated cells. Pancreatic cancer starts with cells carrying KRAS mutations; however, it is not clear how some KRAS mutant cells override cell elimination mechanisms to survive in tissues. **METHODS:** An in vivo mouse model of sporadic tumorigenesis was used to induce *Kras* and/or *Tp53* mutations in low numbers of cells in the adult pancreas. The mutant cell fate was monitored over time using quantitative fluorescence imaging. Gene signatures of noneliminated mutant cell populations were identified using bulk RNA sequencing. Differential gene expression was overlapped with publicly available datasets. Key molecular pathways were validated in murine pancreas using immunofluorescence and functionally tested using inhibitor studies in vivo and epithelial coculture systems in vitro. **RESULTS:** Although most genetically mutant cells are eliminated from the adult pancreas, a population of KRASG12D- or p53R172H-expressing cells are stably retained. Wnt5a signaling, cell dormancy, and stemness were identified as key features of surviving KrasG12D cells in vivo. Wnt5a specifically inhibits apical extrusion of RasV12 cells by promoting stable E-cadherin–based cell–cell adhesions at RasV12: normal cell–cell boundaries in vitro. In the pancreas, Wnt signaling, E-cadherin, and β-catenin are increased at cell–cell contacts between noneliminated KrasG12D cells and normal neighbors. Active Wnt signaling is a general mechanism required to promote KrasG12D and p53R172H cell retention and cell survival in vivo. **CONCLUSIONS:** RAS mutant cells activate Wnt5a and cell dormancy to avoid cell expulsion and to survive in the adult pancreas.

Keywords: Early Tumorigenesis; Pancreatic Cancer; Epithelial Homeostasis; Cell Extrusion; Cell Competition; Oncogenic *RAS*; Wnt5a; Cell Dormancy.

Epithelial tissues are continuously exposed to mutational insults and, as a result, genetically mutant cells often arise in a tissue. Most human cancers start sporadically from epithelial cells carrying genetic mutations that activate oncogenes or inactivate tumor suppressor function. Remarkably, epithelial tissues protect against tumorigenesis by actively removing genetically mutant cells.[1] In general, genetically different cells compete for survival in tissues, resulting in the elimination of "less fit" mutant cells via apoptosis, extrusion, and/or cell differentiation.[1] Under certain conditions,[2,3] competition is tipped in favor of mutant cells. This is better understood in rapidly

Abbreviations used in this paper: **DMSO, dimethyl sulfoxide; FFPE, formalin-fixed, paraffin-embedded; GSEA, gene set enrichment analysis; MDCK, Madin-Darby Canine Kidney; PanIN, pancreatic intraepithelial neoplasia; PBS, phosphate-buffered saline; p.i., post induction; si, small interfering.**

0016-5085
https://doi.org/10.1053/j.gastro.2025.02.042

WHAT YOU NEED TO KNOW

BACKGROUND AND CONTEXT

The adult pancreas actively eliminates KRAS-expressing cells, preventing the occurrence of preneoplasia. KRAS mutations are required at all stages of pancreatic cancer; however, it is not clear how some KRAS mutant cells override cell elimination mechanisms to survive

NEW FINDINGS

Activation of Wnt5a pathway and cell dormancy prevent KRAS cell expulsion from the tissue. Wnt5a signaling promotes stable cell–cell adhesions between KRAS mutant cells and normal neighbors, allowing mutant cells to be stably retained in the tissue.

LIMITATIONS

Future studies are needed to determine the upstream regulators of Wnt5a and cell dormancy.

CLINICAL RESEARCH RELEVANCE

Inhibition of Wnt5a and/or disruption of cell dormancy could provide new strategies to prevent pancreatic tumour initiation and promote tissue health. By understanding the biology of these initial stages of disease will lead to the development of new early detection tools/biomarkers for pancreatic cancer.

BASIC RESEARCH RELEVANCE

Genetically mutant cells activate Wnt5a and cell dormancy to override homeostatic tissue controls, which would otherwise rid tissues of mutant cells. Activation of Wnt5a and a dormant cell state occurs early in cancer development, before preneoplastic growth, to promote survival of cancer-causing cells in a competitive tissue environment.

proliferating tissues that are actively replenished via defined stem cell compartments; tumor risk increases when stem cells acquire genetic mutations that confer a competitive advantage over wild-type counterparts.[4–6] In contrast, our understanding of how competition outcomes shape tumorigenesis in slow proliferating adult tissues that lack a bona fide stem cell compartment remains poorly detailed.

In the pancreas, we recently demonstrated that cells expressing oncogenic *Kras* (*Kras*^{G12D}) are outcompeted by healthy neighbors and are eliminated from exocrine and endocrine epithelial compartments.[7] We have previously described how interactions with normal cells trigger robust evolutionary conserved cell biology phenotypes in *Ras* transformed cells, resulting in the elimination of the mutant cells via cell segregation and cell extrusion.[7–10] Removal of KrasG12D cells from adult pancreas tissues requires local remodeling of E-cadherin–based cell–cell adhesions at normal–mutant boundaries and dynamic changes in mutant and normal cell volume.[7] Importantly, we demonstrated that abrogation of KrasG12D cell elimination in the pancreas significantly increased the appearance of preneoplastic lesions,[7] suggesting cell competition and the subsequent expulsion of mutant cells are disease preventative.

Activating mutations in oncogenic *RAS* is the principal driver gene event in human pancreatic ductal adenocarcinoma,[11] the most common type of human pancreatic cancer. *KRAS* mutations are detected in >90% of human tumors and in vivo mouse studies have found that KRAS signaling is essential for disease to progress through all stages.[12] Missense mutations in *TP53* are the second most common mutation detected in approximately 70% of human pancreatic ductal adenocarcinoma[13] and required for metastasis.[14] How genetically mutant cells survive and grow in the competitive environment of the adult pancreas remains unclear. We sought to understand the mechanisms underpinning how mutant cells avoid cell expulsion and survive in the adult pancreas.

Methods

Mouse Lines, Induction of Cre Recombinase In Vivo, Inhibition of Wnt Pathway In Vivo

Animals were housed in conventional pathogen-free animal facilities and experiments were conducted in accordance with UK Home Office regulations (ASPA 1986 and EU Directive 2010) under the guidelines of Cardiff University Animal Welfare and Ethics Committee. *Pdx1-Cre*^{ERT}; *LSL-Kras*$^{G12D/+}$[15]; *LSL-Trp53*$^{R172H/+}$[16]; *Rosa26*$^{LSL\text{-}tdRFP}$[17] male and female 6- to 8-week-old mice were induced by intraperitoneal injection of tamoxifen in corn oil (low dose: 1 μg/40 g bodyweight once; megadose: three 9 mg/40 g injections[4]). Wnt signaling inhibition followed low-dose tamoxifen schedule; mice were aged to 35 days post induction (p.i.) and treated with WNT-974 Q11 (Stratech) 1.5 mg/kg or vehicle (dimethyl sulfoxide [DMSO]) in corn oil by oral gavage 5 d/wk for 4 weeks.

RNA Sequencing

Sequenced reads Fastq files were quality checked using FastQC software (Babraham Bioinformatics). Reads were Q12 aligned to the mouse genome using the STAR package, and reads were counted using the FeatureCounts package, after removing duplicates using the MarkDuplicates tool (GATK). Differential expression was normalized and calculated using DESeq2 package, comparing different genotypes against control. Gene set enrichment analysis (GSEA) software, version 4.2.2 (Broad Institute) was used for pathway enrichment analysis and Prism software, version 10.0.2 (GraphPad) was used for heatmap graphs and normalized enrichment score graphs (GEO ID: GSE255283).

Tissue Staining

Pancreas was harvested at specified time points and fixed in 10% neutral buffered formalin overnight at 4°C, before dissection into 2 pieces (head-body and body-tail) and embedded in either paraffin or OCT embedding matrix. Formalin-fixed paraffin-embedded (FFPE) pancreas was sectioned (7-μm thickness) and stained with anti-RFP, anti–cleaved caspase-3, and anti–Ki-67 staining were performed via immunohistochemistry in FFPE tissue sections. Tissues sections were dewaxed and rehydrated. For antigen retrieval, tissue sections were incubated for 15 minutes at 37°C in 20 μg/mL Proteinase K diluted in Tris-buffered saline with Tween 20 Q13 or boiled in citrate buffer pH 6 for 15 minutes (Supplementary Table 14). Tissues were then blocked with 3% H_2O_2 for 20 or

10 minutes at room temperature (depending on the antigen retrieval method) and 5% NGS Tris-buffered saline with Tween 20 for 60 minutes at room temperature. Sections were incubated overnight at 4°C with the primary antibody diluted in 5% NGS Tris-buffered saline with Tween 20 (Supplementary Table 14). Tissues were stained with the secondary antibody ImmPRESS goat anti-rabbit (MP-7451, Vector Laboratories) for 60 minutes at room temperature, followed by 3,3′-diaminobenzidine tetra hydrochloride chromogen (peroxydase substrate kit, Vector Laboratories). Sections were dehydrated and mounted with DPX (Sigma-Aldrich). Immunofluorescence co-staining using either anti-CD44 and anti-RFP (Rockland) was performed in FFPE tissue slices using the same antigen retrieval and primary antibody incubations as described for immunohistochemistry, followed by Alexa Fluor secondary antibody incubation for 60 minutes at room temperature and Hoechst (ThermoFisher) (Supplementary Table 14) and mounted using Mowiol (Sigma-Aldrich).

For β-catenin, E-cadherin, K-cadherin, and RFP (Creative Diagnostics) immunofluorescence staining, pancreas was embedded in butyl-methyl methacrylate plastic under UV after dehydration and resin infiltration.[7,18] Tissue was sectioned in 2-μm-thick slices and rehydrated. Tissue staining followed the same protocol as immunofluorescence in FFPE sections.

Pancreas embedded in OCT embedding matrix was sectioned (10-μm thickness), permeabilized with 0.05% sodium dodecyl sulfate (Sigma-Aldrich) and 0.05% Triton X100 (Sigma-Aldrich) solution, blocked with phosphate-buffered saline (PBS) with Tween 20 (0.01% Triton X100) and stained with anti-p27, anti-Wnt5a, anti-Dvl2 and anti-Sox9 primary antibodies for 2 hours at room temperature, Alexa Fluor secondary antibody incubation for 60 minutes at room temperature and Hoechst (ThermoFisher) and mounted using Mowiol (Sigma-Aldrich). Antibody details are detailed in Supplementary Table 14.

Global levels of endogenous RFP were measured in 10-μm formalin-fixed OCT frozen sections, as described previously.[7] RFP-positive area was averaged from 3 tissue slices per mouse separated by at least 20 μm between each section.

To assess the presence of pancreatic intraepithelial neoplasia (PanIN) lesions, FFPE sections were stained with Alcian blue, as described previously.[7] β-galactosidase activity was determined using the Senescence β-galactosidase Staining Kit (9860, Cell Signaling) using the manufacturer's instructions.

Madin-Darby Canine Kidney Cell Lines and In Vitro Experiments

For extrusion assays, Madin-Darby Canine Kidney (MDCK)-pTR GFP–RasV12 cells were combined with parental MDCK cells at a 1:50 ratio and induced using tetracycline, as described previously.[7,9] For Wnt signaling experiments, GFP-RasV12 cells were treated with PBS, Wnt3a (1 μg/mL), or Wnt5a (100 ng/mL) 2 hours post-tetracycline induction.

c-Myc was silenced in tetracycline-induced GFP-RasV12 cells by transfection with 100 ng si (small interfering) RNA oligos targeting *Myc* (see Supplementary Material). GFP-RasV12 cells were mixed with parental MDCK cells 24 hours after transfection and fixed after an additional 48 hours

For Wnt pathway inhibition, GFP-RasV12-expressing cells were transfected with siMyc1+2/siScr or treated with recombinant Wnt5a/PBS for 24 hours and then mixed with parental cells. Wnt5a treatment was maintained during the whole experiment. WNT-974 (Stratech, 1 μM) or *OMP*-18R5 (10 mg/mL) was added to the medium 8 hours after GFP-RasV12 and parental cells were mixed.

Confrontation assays and migration speed analysis were carried out as described previously.[3] siMyc/siScr-GFP-RasV12 cells were plated 24 hours after transfection and inserts were removed 8 hours after. Cells were treated with PBS/Wnt5a for 8 hours before inserts were removed. PBS/Wnt5a treatment was maintained during the whole experiment. WNT-974/DMSO was added when inserts were removed.

Pancreatic Ductal Epithelial Cell Co-Culture Assays

Harvesting and culture of nontransformed pancreatic ductal epithelial cells, cell–cell mixing, and immunostaining was carried out as described previously.[7] Transformed tumor-derived epithelial cells obtained from KC mice (KrasG12D-expressing ductal epithelial cells) were treated with PBS or recombinant Wnt5a for 24 hours, before being prelabeled with CMFDA Green CellTracker dye (ThermoFisher Scientific) 1:1000 for 1 hour at 37°C. PBS/Wnt5a was maintained in the medium; 12 hours after plating cells were treated with DMSO or WNT-794 (Stratech, 1 μM) for 36 hours. Cells were fixed and stain using anti–E-cadherin antibody (BD Biosciences).

Statistical Tests

Statistical analyses were performed using Prism software, version 10.0.2. Normally distributed data, as determined by the Shapiro-Wilke test or D'Agostino and Pearson test were analyzed using unpaired Student *t* tests. A P value of $< .05$ was considered as significant and a rejection of the null hypothesis. Graphical data represent mean ± SD. Gene sets were considered enriched if they had a false discovery rate of <0.25. Heatmaps were created by computing normalized gene counts for each individual sample into row *z* scores.

Additional methods are described in Supplementary Material.

Results

Cells Expressing KrasG12D or p53R172H Mutations Are Eliminated From Adult Pancreas

Co-expression of both mutations in the same cell abrogates cell elimination in vivo. To model sporadic pancreatic cancer, we used the following pancreas-specific genetically engineered mouse models: KC: *Pdx1-Cre*^{ERT}; *LSL-Kras*$^{G12D/+}$; *Rosa26*$^{LSL\text{-}tdRFP}$; PC: *Pdx1-Cre*^{ERT}; *LSL-Trp53*$^{R172H/+}$; *Rosa26*$^{LSL\text{-}tdRFP}$; and KPC: *Pdx1-Cre*^{ERT}; *LSL-Kras*$^{G12D/+}$; *Trp53*$^{R172H/+}$; *Rosa26*$^{LSL\text{-}tdRFP}$. Our experimental control was *Pdx1-Cre*^{ERT}; *Rosa26*$^{LSL\text{-}tdRFP}$ mice (Figure 1*A*, *left*). Adult mice were treated with low-dose tamoxifen and aged for 7, 35, or 70 days p.i. (Figure 1*A*, *right*).[7] To monitor cell fate, we measured RFP levels over time. Consistently,[7] we found that low-dose tamoxifen induced stochastic RFP labeling in approximately 20%–25% of the tissue in all genotypes (Figure 1*B* and *C*). RFP fluorescence significantly decreased in KC and PC tissues, and it did not significantly change in double-mutant (KPC) tissues from 7 to 35/70 days p.i. (Figure 1*B* and *C*). Pancreas tissue histology was

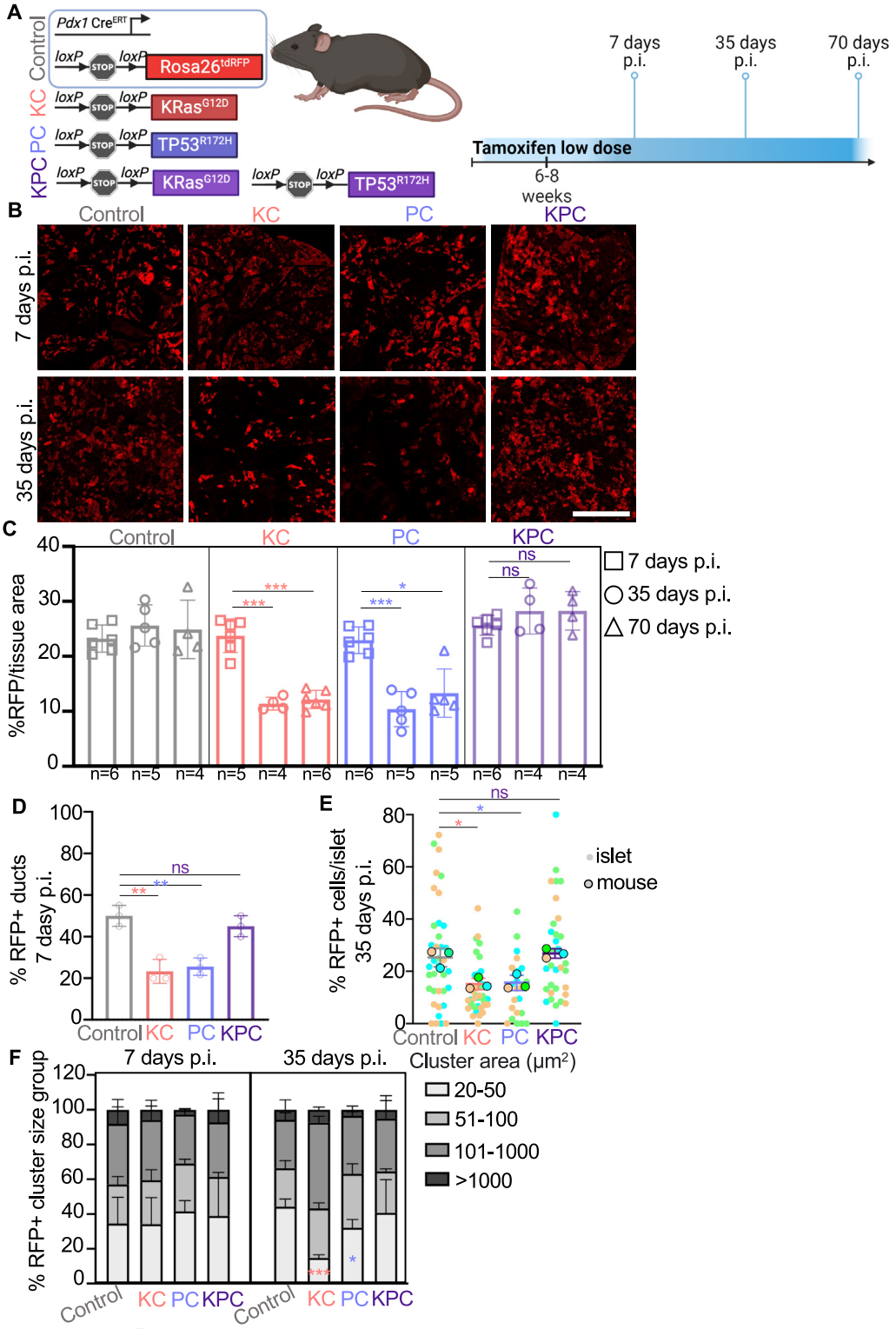

Figure 1. Cells expressing p53R172H are eliminated from adult pancreas in vivo. Coexpression of p53R172H mutations prevents KrasG12D cell elimination in vivo. (*A*) *Schematic* of mouse models (*left*), tamoxifen treatment and time points (*right*). (*B*) Representative *images* of endogenous RFP fluorescence. *Scale bar:* 500 μm. (*C*) Percentage of RFP fluorescence per total tissue area. N = numbers described in the graph. (*D*) Percentage of RFP$^+$ ducts at 7 days p.i. (n = 3 mice). (*E*) Percentage of RFP$^+$ cells per total number of cells in islets at 35 days p.i. (n = 3 mice). (*F*) Percentage of RFP$^+$ clusters grouped according to cluster area (mm^2). Control, KrasG12D (KC), p53R172H (PC), double mutant (KPC). Data represent mean ± SD. Student *t* tests were used to analyze the data. *$P < .05$; **$P < .001$; ***$P < .0001$.

unaffected by low-level transgene expression (Supplementary Figure 1*A*). Because exocrine acinar cells comprise >90% of the adult pancreas, these data suggest that changes in global RFP fluorescence reflect changes in RFP^+ acinar cell populations over time. RFP^+ ducts were significantly less frequent in KC and PC tissues 7-day p.i. compared with control, while number of RFP^+ ducts in KPC tissues was comparable to controls (Figure 1*D*). The percentage of RFP^+ cells per islet significantly decreased in KC and PC tissues, whereas the frequency of RFP^+ cells per islet in KPC tissues was comparable to wild-type controls (Figure 1*E*). We have previously shown that KrasG12D cells are competitively eliminated at cell boundaries with surrounding normal cells, resulting in the elimination of small clusters.[7,19] The percentage of small clusters (<50 μm^2) significantly decreased in KC and PC tissues over time, while no significant differences were found in KPC tissues, compared with controls (Figure 1*F*), suggesting KPC cells do not respond to cell–cell interactions with normal cells. Thus, like KrasG12D-expressing cells,[7] p53R172H single mutant cells are eliminated from all epithelial compartments. Cells expressing both KrasG12D and p53R172H mutations are not eliminated from endocrine/exocrine epithelial tissues.

Transcriptional Profiles of Noneliminated Mutant Cells Indicate Activation of Pro-Survival Signals

We consistently found that approximately 10% of tissue area remains RFP-labeled in KC (KrasG12D) and in PC (p53R172H) tissues post the 35-day time point[7] (Figure 1*B* and *C*), indicating that some mutant cells are not eliminated from the pancreas in vivo. We found rare Alcian blue–positive lesions[7] in 6 of 9 KC mice at 168 days p.i. (Supplementary Figure 1*B*), suggesting some noneliminated KrasG12D cells progress to PanINs. No PanIN lesions were detected in PC tissues. PanIN lesions were detected more frequently in 5 of 5 KPC tissues (Supplementary Figure 1*B*) and 4 of 5 KPC mice developed tumors by 168 days p.i.

To identify gene signatures of noneliminated mutant cells and determine whether common pathways are activated by all mutant cells, we performed bulk RNA sequencing (Figure 2*A*). Whole pancreata were harvested from experimental cohorts (KC/PC/KPC/control) at 35 days p.i. We used anti-leptin antibodies to enrich for acinar/ductal epithelial cells and fluorescence-activated cell–sorted $leptin^+$ RFP^+ cells for RNA sequencing (see Supplementary Methods). We assumed that most RFP^+ cells isolated for RNA sequencing are acinar in origin as RFP^+ ductal cells are rare at 7 days p.i. (Figure 1*D*). We compared differential gene expression in noneliminated mutant cells to wild-type controls. Unsupervised principal component analysis (Supplementary Figure 2*A*) and unsupervised clustering heatmaps of normalized differentially expressed genes (Supplementary Figure 2*B*) showed distinct transcriptional profiles for RFP^+ cell populations of each genotype. In general, KC cells up-regulated genes, whereas PC and KPC cells down-regulated genes compared to wild-type controls (Supplementary Tables 1–3).

To elucidate the biological pathways underpinning mutant cell retention in pancreas tissues, we applied GSEA (GSEA Hallmarks, KEGG MEDICUS databases). We generated normalized enrichment scores with *P* values adjusted using false discovery rate of <0.25 to rank statistically significant gene sets enriched in KC, PC, or KPC transcriptomes compared to wild-type controls. KC, PC, and KPC (Figure 2*B* and *C*, Supplementary Figure 2*C–F*, 2*G*) signatures deregulated Kras, MAPK, and p53 signaling pathways, suggesting deregulation of Kras signaling and/or p53 pathway is a general requirement for mutant cells to remain in tissues. KC signatures positively enriched for pro-survival and protumorigenic pathways (eg, epithelial to mesenchymal transition, tumor necrosis factor–α signaling, hypoxia, angiogenesis, Notch signaling, and Wnt signaling) and immune response (eg, Il2-Stat5 signaling and tumor necrosis factor–α via nuclear factor κB signaling) (Figure 2*B*). Gene signatures from both PC (Figure 2*C*) and KPC (Supplementary Figure 2*G*) negatively enriched for apoptosis pathways and inflammatory responses, suggesting cell survival is a requisite for retention of mutant cells in tissues.

Gene Signatures of Noneliminated Krasg12d Cells Correlate With Pancreatic Ductal Adenocarcinoma Initiation and With Increased Stemness and Cellular Reprogramming

KRAS mutations are detected in the majority of human pancreatic ductal adenocarcinoma tumors and are required to drive all stages of pancreatic cancer.[12] Thus, we focused our analyses on understanding how KrasG12D cells avoid cell elimination. Expression of oncogenic *Kras* in the pancreas triggers injury and stress responses, which often translate as cellular reprogramming and changes in cell fate.[20,21] KC signatures positively correlated with WP_Pancreatic_Adenocarcinoma_Pathway in GSEA analysis contrary to PC and KPC signatures (Supplementary Figure 2*H–J*). A consistent up-regulation of pancreas stem and progenitor genes (eg, *Nkx6-1*, *Prom-1*, *Hnf1b*)[22] was observed in noneliminated KC signatures (Figure 3*A*). Canonical markers of Q16 spasmolytic polypeptide-expressing metaplasia[22] were up-regulated in noneliminated KC cells (Supplementary Figure 3*A*), as well as acinar, ductal, and mucin genes (Supplementary Figure 3*B*). Stemness gene signatures enriched in KC signatures compared with wild-type control, contrary to PC and KPC signatures (Supplementary Figure 3*A–I*). Gene signature data imply that noneliminated KrasG12D populations represent differentiated acinar cells and early embryonic pancreatic progenitors, cells undergoing acinar–ductal metaplasia and gastric pyloric and intestinal metaplasia, all of which are evident in tissues at very early time points.

Noneliminated KrasG12D Mutant Cells Express Features of Cell Dormancy

Analysis of RFP levels in tissues over time (Figure 1*C*) indicated that noneliminated cells are not actively dividing

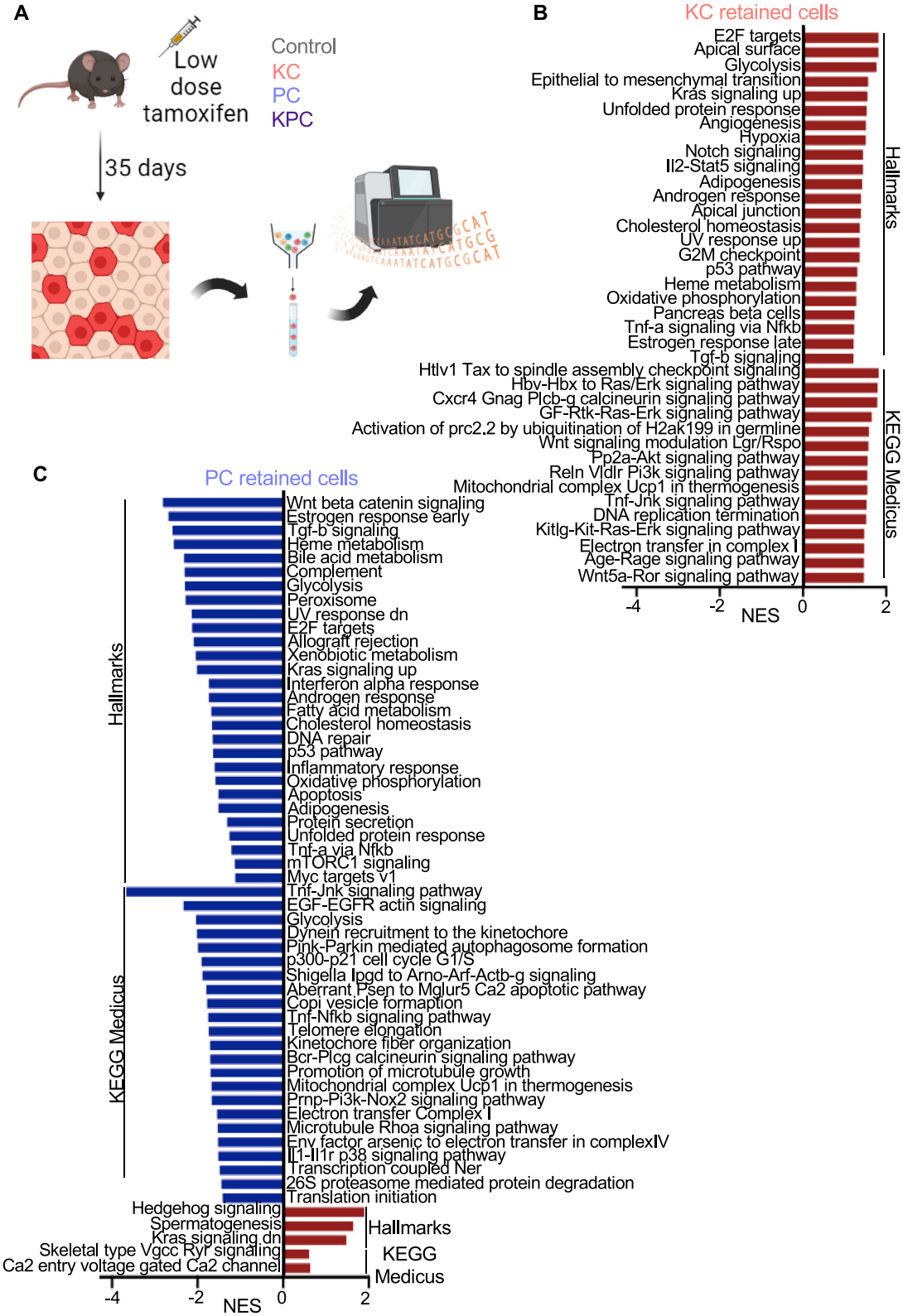

Figure 2. RNA sequencing results indicate cell fate changes in p53R172H and KrasG12D mutant retained cells. (*A*) Experimental design for tissue collection for RNA sequencing. (*B, C*) Normalized enrichment scores (NES; false discovery rate <0.25) of GSEA on the Hallmarks and KEGG MEDICUS gene sets for the RNA sequencing analysis of (*B*) KC retained cells or (*C*) PC retained cells. Full list of genes can be found in Supplementary Tables 4–7.

print & web 4C/FPO

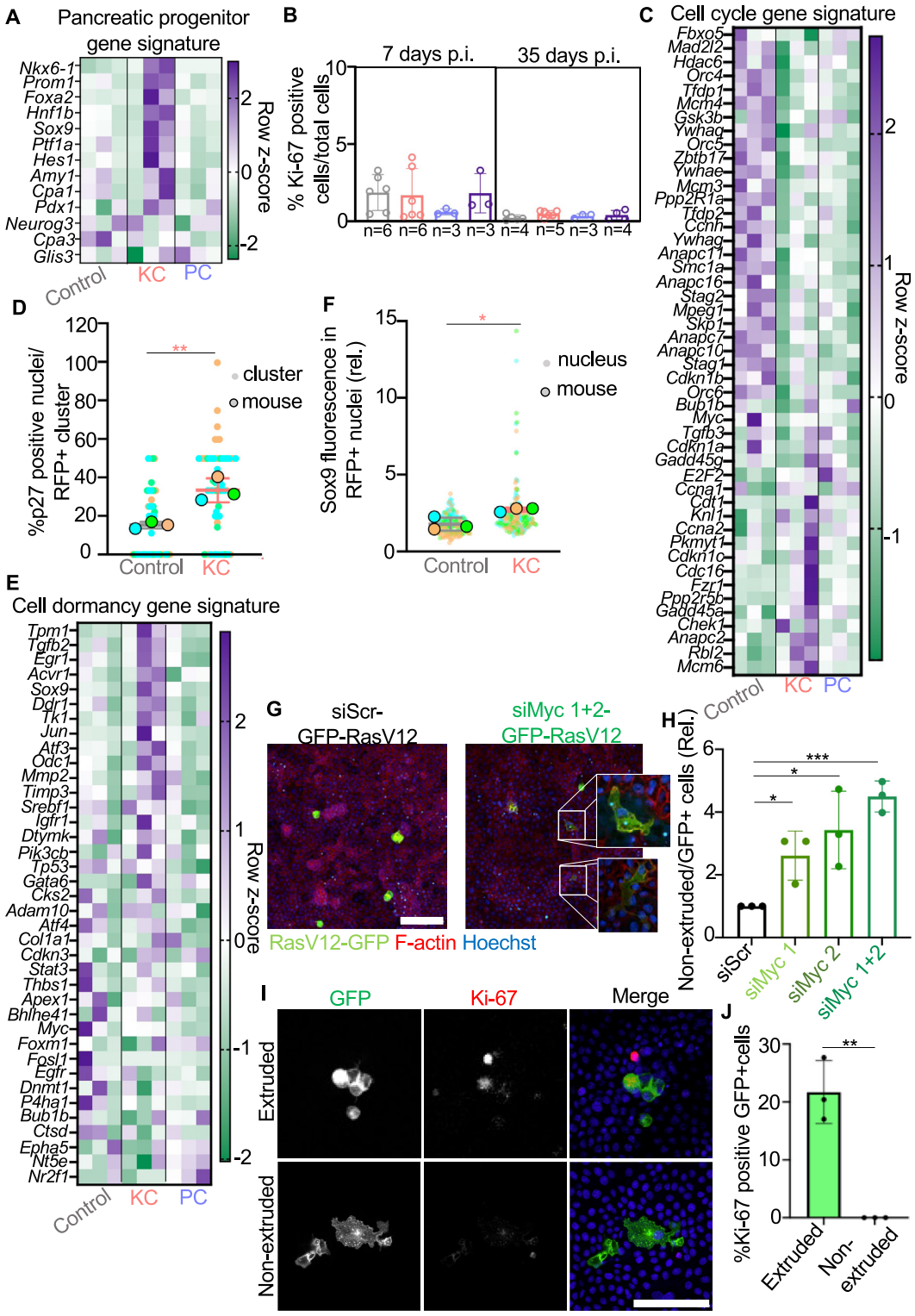

Figure 3. Cell dormancy/diapause gene signatures and cell cycle arrest are features of noneliminated Ras mutant cells. *Heatmaps* show row *z* scores of (*A*) pancreatic progenitor associated[23] (*C*) cell cycle (KEGG M7963) associated and (*F*) cell dormancy[22] gene signatures. Full list of genes can be found in Supplementary Table 10. (*B, D*) Percentage of Ki-67–positive cells/total cells. N = numbers described in graph. (*D*) Percentage of p27 positive nuclei/total nuclei in each RFP$^+$ cluster (n = 3 mice). (*F*) Mean fluorescence intensity relative to background of Sox9 per nuclei of RFP$^+$ cells (n = 3 mice). (*G, I*) Confocal *images* of cell extrusion experiment. *Scale bar:* 100 μm. (*H*) Proportion of nonextruded GFP-RasV12 cells relative to non-extruded siScr-GFP-RasV12 cells (n = 3 experiments). (*J*) Percentage of Ki-67–positive cells extruded GFP-RasV12 cells of total extruded cells (n = 3 experiments). siScr, scrambled siRNA; siMyc1+2, two siRNA oligos targeting endogenous *Myc*. Data represent mean ± SD. Student *t* tests were used to analyze the data. *$P < .05$; **$P < .001$; ***$P < .0001$.

in tissues. We found no evidence of cell senescence (β-galactosidase activity; Supplementary Figure 4*A*) or increased caspase-3–positive events (Supplementary Figure 4*B*) in 35-day KC pancreas tissues, suggesting a general absence of apoptosis. KC transcriptomes negatively correlated with oxidative stress response pathways (GOBP_RESPONSE_TO_OXIDATIVE_STRESS, M3223; Supplementary Figure 4*C*). PC and KPC (Supplementary Figure 4*D* and *E*) gene signatures positively correlated with oxidative stress, suggesting noneliminated mutant p53-expressing populations (PC, KPC) are potentially under oxidative stress, whereas this is unlikely for KC cells. Immunostaining for Ki-67 showed an absence of proliferation in all tissues (Figure 3*B*). GSEA analyses identified enrichment of proliferation-related pathways (eg, E2F targets and GF-Rtk-Ras-Erk signaling) and enrichment of pathways indicative of dysregulation of the cell cycle towards genomic instability (eg, G_2M checkpoint, Htlv Tax to spindle assembly checkpoint, Hbv-Hbx to Ras/Erk signaling, DNA-replication termination)[24] in noneliminated KC cells compared to controls (Figure 2*B*). We observed a general down-regulation of cell cycle genes in KC signatures (Figure 3*C*). Similarly, gene expression profiles of PC cells (Figure 3*C*) and GSEA analyses of mutant p53-expressing cells indicated a general down-regulation of cell cycle and proliferation-related pathways (PC; Figure 2*C*; KPC; Supplementary Figure 2*E*). We scored a significant increase in p27-positive RFP^+ nuclei in KC tissues compared to controls (Figure 3*D*), suggesting noneliminated KrasG12D cells are arrested at the G_1 stage of the cell cycle.[25] Interestingly, noneliminated KC gene signatures were also enriched for pathways associated with cancer cell dormancy (eg, oxidative phosphorylation, unfolded protein response, and hypoxia; Figure 2*B*). Cell dormancy describes a reversible cell cycle arrested state, often triggered by cell stress.[26] Diapause is a temporary halt in embryogenesis when conditions are detrimental to development.[27] Cell dormancy (Figure 3*E*, Supplementary Figure 4*F*) and diapause (Supplementary Figure 4*G*) gene signatures were enriched in noneliminated KC cells compared to control. Using Sox9 as a marker of dormant cells, we found that Sox9 fluorescence was significantly increased in RFP^+ nuclei in KC tissues compared with RFP^+ nuclei in wild-type controls (Figure 3*F*). NRF2 (a transcription factor activated during cell dormancy[28]) pathway and NRF2 target genes (Supplementary Figure 4*H* and *I*) positively enriched in noneliminated KC cells only. Diapause gene signatures were not significantly enriched in PC cells (Figure 3*E*, Supplementary Figure 4*G*). These data infer that noneliminated mutant cells deregulate the cell cycle towards an arrested state; however, 2 copies of functional p53 are required for cells to adopt a dormant or diapaused state.[29–31]

Cell Cycle Arrest Prevents Mutant Cell Extrusion In Vitro

We hypothesized that mutant cells override cell elimination in vivo by arresting in the cell cycle. To test this, we used previously established cell competition assays and MDCK cells expressing GFP-tagged constitutively active oncogenic RasV12 (GFP-RasV12).[8–10] When surrounded by normal MDCK cells, GFP-RasV12–expressing MDCK cells are outcompeted via cell extrusion.[9,10] In contrast, MDCK cells expressing mutant p53 are outcompeted by normal cells via necroptosis.[32] c-Myc is a key regulator of the cell cycle and depletion of Myc triggers cell dormancy.[33] We induced cell cycle arrest in GFP-RasV12 cells via *Myc* knockdown using 2 c-Myc siRNAs (siMyc-GFP-RasV12). Expression of c-Myc siRNA yielded a decrease in Myc and phospho-p38 protein levels, an increase in p21 protein levels (Supplementary Figure 5*A* and *B*) and a marked reduction in GFP-RasV12 cell confluency (Supplementary Figure 5*C*). In cell extrusion assays,[9,10] GFP-RasV12 cells were first transfected with siScr or siMyc oligos and then mixed with normal MDCK cells at 1:50 ratios. The proportion of nonextruded GFP-RasV12 cells significantly increased when GFP-RasV12 cells were depleted for Myc (Figure 3*G* and *H*). Nonextruded siMyc-GFP-RasV12 cells were not proliferating, whereas the minority of Ki-67–positive cells were extruded (Figure 3*I* and *J*). We also used cell confrontation assays[10] and live-cell imaging of normal–mutant interactions across an entire epithelial cell sheet (Supplementary Figure 5*D*). Upon collision with normal MDCK cells, GFP-RasV12 cells are triggered to retract and segregate away from normal cells, separating via the formation of smooth boundaries.[10] GFP-RasV12 cells depleted for Myc (siMyc1+2) retracted less efficiently than GFP-RasV12 siScr controls (Supplementary Figure 5*E* and *F*). Thus, RasV12 cells depleted for Myc and exhibiting cell cycle arrest are not extruded or triggered to segregate by normal cells, suggesting cell cycle arrest protects RasV12 mutant cells from cell elimination.

Noneliminated KrasG12D Cells Activate β-Catenin Independent Wnt Signaling In Vivo

The Wnt pathway positively regulates cancer cell dormancy,[34,35] diapause,[36] and stemness.[37] GSEA analyses identified an enrichment for Wnt pathway activation in noneliminated KC transcriptomes compared to controls (Wnt signaling modulation Lgr/Rspo, Wnt5a-Ror signaling pathway) (Figure 2*B*) and increased expression of Wnt pathway–related genes (Figure 4*A*). Wnt/β-catenin pathway gene expression and signatures were generally down-regulated in KC and PC cells (Figures 2*C* and 4*B*, Supplementary Figure 6*A*). Both KC and PC gene signatures positively correlated with Wnt5a-Ror signaling pathway (Supplementary Figure 6*B* and *C*), and Wnt ligands and receptors associated with Wnt5a-Ror signaling were increased in KC cells (Figure 4*C* and *D*, Supplementary Table 11).

To investigate active Wnt signaling in vivo, we first analyzed expression of CD44 protein, a target of β-catenin–dependent and independent signaling.[38] Consistently,[39] we observed CD44 labeling at cell membranes in PanINs (Supplementary Figure 6*D*). CD44 was significantly increased at RFP^+:RFP^- cell–cell boundaries in KC and PC tissues compared to wild-type controls (Supplementary

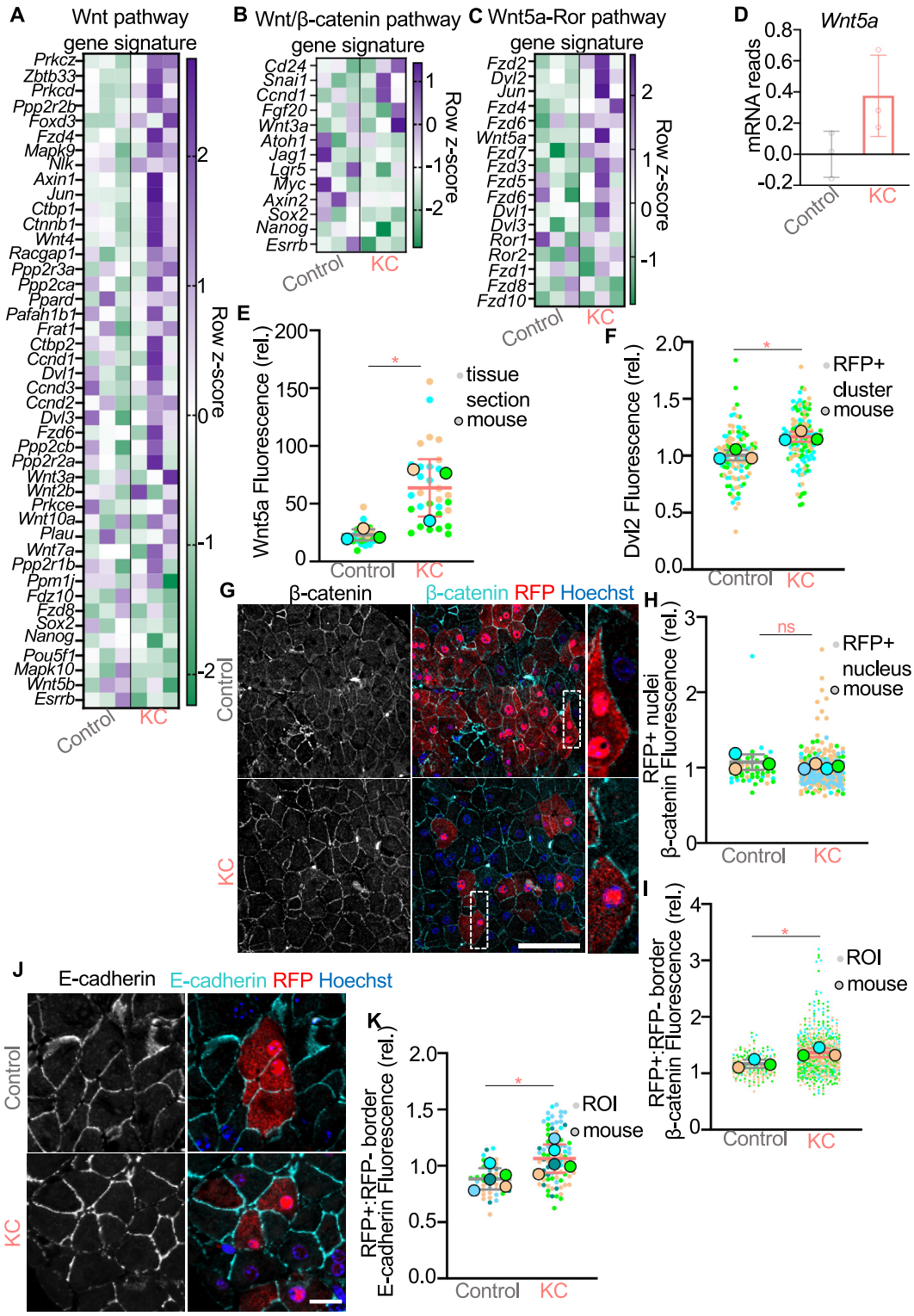

Figure 4. Wnt pathway is activated at normal–mutant cell–cell boundaries in vivo. *Heatmaps* show row *z* scores of (*A*) Wnt signaling pathway (WP_Wnt_signaling MM15829), (*B*) Wnt/β-catenin pathway (Hallmark_Wnt_beta_catenin_signaling MM3864) or (*C*) Wnt5a-Ror pathway (KEGG_Medicus_Wnt5a_Ror_signaling M47823) related genes. (*D*) *Wnt5a* messenger RNA reads relative to control reads obtained from the RNA sequencing experiment (n = 3 samples). (*E, F*) Mean fluorescence intensity relative to background of Wnt5a (*E*) or Dvl2 (*F*) (n = 3 mice). (*G*) Representative images of RFP and β-catenin staining. *Scale bar*: 50 μm. (*H, I*) Mean fluorescence intensity relative to background of β-catenin in the nuclei of RFP$^+$ cells (*H*) or at the boundary between RFP$^+$:RFP$^-$ cells (*I*) (n = 3 mice). (*J*) Confocal *images* of pancreas tissues stained with anti-RFP and anti–E-cadherin. *Scale bar:* 20 μm. (*K*) Mean fluorescence intensity relative to background of E-cadherin at the boundary between RFP$^+$:RFP$^-$ cells (n = 5 mice). Data represent mean ± SD. Student *t* tests were used to analyze the data. *$P < .05$.

Figure 6*E*. *F*, and *H*). In contrast, CD44 was significantly reduced within a cluster of KC and PC cells (Supplementary Figure 6*E*, *G*, and *I*). We compared CD44 levels in tissues where KrasG12D cells are not competitively eliminated (high dose of tamoxifen-KC megadose)[7] and found CD44 levels were significantly lower at mutant–normal cell boundaries in KC megadose tissues compared to KC low-dose tissues (Supplementary Figure 6*E* and *F*), and significantly higher between KC cells (Supplementary Figure 6*E* and *G*). We observed significant increase in Wnt5a (Figure 4*E*) and Dvl2 (Figure 4*F*) protein in KC cells relative to controls, suggesting Wnt5a signaling is active in non-eliminated KrasG12D cells in vivo. Nuclear β-catenin was undetectable in both control and KC cells (Figure 4*G* and *H*), indicating that Wnt/β-catenin signaling is not active in noneliminated KC cells, consistent with our transcriptional analysis. Instead, β-catenin was significantly increased at RFP^+:RFP^- cell–cell contacts in KC tissues compared to controls (Figure 4*G* and *I*). Moreover, E-cadherin was also significantly elevated at RFP^+:RFP^- boundaries in KC tissues compared to controls (Figure 4*J* and *K*). We also detected increased messenger RNA expression of atypical *cadherin-6* (Supplementary Figure 7*A*) and increased protein levels (K-cadherin) in KC cells (Supplementary Figure 7*B* and *C*). Together, our data suggest that β-catenin–independent Wnt signaling is active in vivo and Wnt signaling increases cohesiveness and/or stability of E-cadherin-based cell–cell adhesions at cell–cell boundaries between noneliminated KrasG12D cells and normal neighbors.

Wnt5a Inhibits RasV12 Cell Extrusion In Vitro by Stabilizing E-Cadherin–Based Cell–Cell Adhesions

To establish whether Wnt5a directly inhibits RAS mutant cell elimination, we returned to MDCK cell extrusion assays.[9,10] The proportion of nonextruded GFP-RasV12 cells significantly increased in the presence of Wnt5a compared with PBS-treated controls (Figure 5*A* and *B*). Remarkably, addition of Wnt3a had no effect on RasV12 cell extrusion rates (Figure 5*A* and *B*), suggesting only β-catenin–independent Wnt signaling inhibits RasV12 cell extrusion.

Cell extrusion requires dynamic remodeling of E-cadherin–based cell–cell adhesions at normal–mutant cell–cell boundaries.[9,40,41] E-cadherin and β-catenin staining was more defined and significantly increased at normal–mutant cell–cell contacts in Wnt5a-treated cells compared to PBS-treated controls (Figure 5*C*–*E*). In contrast, Wnt3a treatment had no significant effect on E-cadherin or β-catenin at RasV12–normal cell–cell contacts; instead, E-cadherin/β-catenin was diffuse/weak and sometimes absent, like controls (Figure 5*D* and *E*). Treatment with Wnt5a significantly increased the levels of E-cadherin (Supplementary Figure 7*D*), but had no effect on β-catenin levels (Supplementary Figure 7*E*) detected at cell–cell contacts between RasV12 cells, suggesting Wnt5a signaling specifically modulates E-cadherin at cell–cell contacts. Addition of Wnt3a had no statistically significant effect on E-cadherin or β-catenin at cell–cell contacts between RasV12 cells (Supplementary Figure 7*D* and *E*). In cell confrontations assays,[10] Wnt5a treatment significantly reduced RasV12 cell speed compared to PBS-treated controls, whereas normal MDCK cell speed was unaffected (Supplementary Figure 7*F*), implying Wnt5a signaling specifically affects RasV12 cell cohesion.

E-cadherin endocytosis is required for apical extrusion of RasV12 cells from normal MDCK cell sheets.[41] Before cell extrusion events (16 hours),[41] E-cadherin staining was weakly visible/diffuse at RasV12–normal cell–cell contacts in PBS-treated controls and was often detected in distinct intracellular puncta in both RasV12 and normal cells (Figure 5*F*). In contrast, Wnt5a-treated cells showed strong, defined E-cadherin at cell–cell contacts and E-cadherin–positive puncta were less visible in RasV12 cells and neighboring cells, which was reflected in a significant reduction in fluorescence intensity (Figure 5*F* and *G*). Caveolin-1 (a key regulator of endocytosis and cell extrusion[42]) fluorescence was significantly reduced at RasV12–normal cell–cell contacts in Wnt5a-treated cells compared with PBS controls (Supplementary Figure 7*G* and *H*), suggesting Wnt5a treatment blocks E-cadherin recycling/endocytosis at RasV12–normal boundaries. Together, our data showed that Wnt5a stabilizes E-cadherin–based cell–cell adhesion at normal–mutant boundaries potentially by preventing E-cadherin internalization, which correlates with a significant reduction in RasV12 cell extrusion and increase in RasV12 cell cohesion.

Wnt Signaling Is Required to Promote Retention of Mutant Cells In Vitro and In Vivo

Next, we set out to test whether Wnt signaling is required to prevent mutant cell elimination. In MDCK cells, overexpression of RasV12 induces expression and secretion of Wnt5a in a porcupine-dependent manner.[43] Porcupine is an acyltransferase enzyme required for the lipidation and trafficking of Wnt proteins.[44] We observed a significant reduction in the proportion of nonextruded siMyc 1+2-GFP-RasV12 cells from normal monolayers treated with porcupine inhibitor WNT-974, compared to DMSO-treated co-cultures (Figure 6*A* and *B*). In cell confrontation assays,[10] WNT-974–treated siMyc 1+2-GFP-RasV12 cells efficiently retracted and segregated from normal cells with a smooth boundary (Supplementary Figure 8*A*–*C*), compared with DMSO-treated cells.

The effects of Wnt5a on RasV12 cell extrusion rates were reversed in the presence of WNT-974 (Figure 6*C* and *D*) or the Frizzled receptor antagonist OMP-18R5[39] (Figure 6*C* and *E*) compared with DMSO-treated controls. Wnt5a induced a significant decrease in the level of intracellular E-cadherin fluorescence in RasV12 cells, which was rescued in the presence of WNT-974 (Figure 6*F* and *G*), implying that Wnt signaling is required to prevent E-cadherin internalization and endocytosis. In cell confrontation assays, Wnt5a treatment significantly decreased RasV12 cell speed, and this significantly increased in the presence of WNT-974 (Supplementary Figure 8*D*). We repeated coculture experiments using primary murine pancreatic ductal

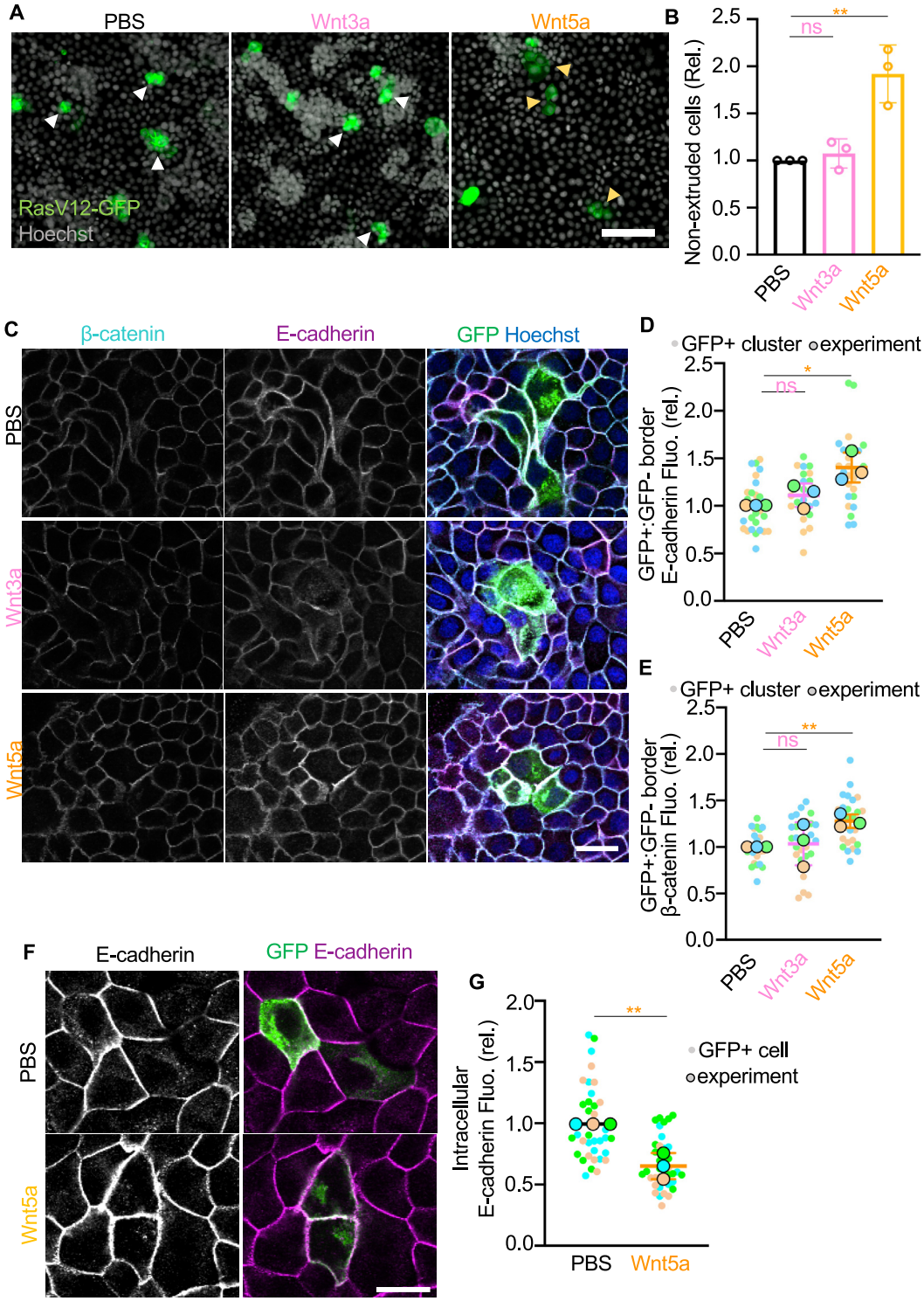

Figure 5. Wnt5a induces stable E-cadherin–based cell–cell adhesion in RasV12 cells. (*A*) Confocal images of cell extrusion experiment. *Scale bar:* 100 μm. (*B*) Proportion of nonextruded GFP-RasV12 cells relative to nonextruded PBS-treated GFP-RasV12 cells (n = 3 experiments). (*C, F*) Confocal *images* of GFP-RasV12 cells mixed with MDCK cells 48 hours (*C*) or 16 hours (*F*) after treatment. *Scale bar:* 20 μm. (*D, E*) Mean fluorescence intensity of E-cadherin (*D*) or β-catenin (*E*) at the boundary between GFP-RasV12 and MDCK cells relative to PBS-treated cells (n = 3 experiments). (*G*) Mean fluorescence intensity of intracellular E-cadherin in GFP-RasV12 relative to PBS-treated cells (mixed with MDCK cells; n = 3 experiments). Data represent mean ± SD. Student *t* tests were used to analyze the data. $^{*}P < .05$; $^{**}P < .001$.

epithelial cells.[7] When mixed with nontransformed pancreatic ductal epithelial cells, prelabeled KRasG12D-expressing ductal epithelial cells are often visible on the apical surface of the underlying nontransformed cells (Supplementary Figure 8*E*). Treatment with Wnt5a significantly increased the number of KrasG12D-exxpressing cells integrated into the monolayer (Supplementary Figure 8*E* and *F*). This effect of Wnt5a was significantly reduced in the presence of WNT-974 (Supplementary Figure 8*E* and *F*). Consistent with MDCK experiments, Wnt5a treatment induced a significant reduction in the level of intracellular E-cadherin fluorescence in KrasG12D ductal epithelial cells, which was

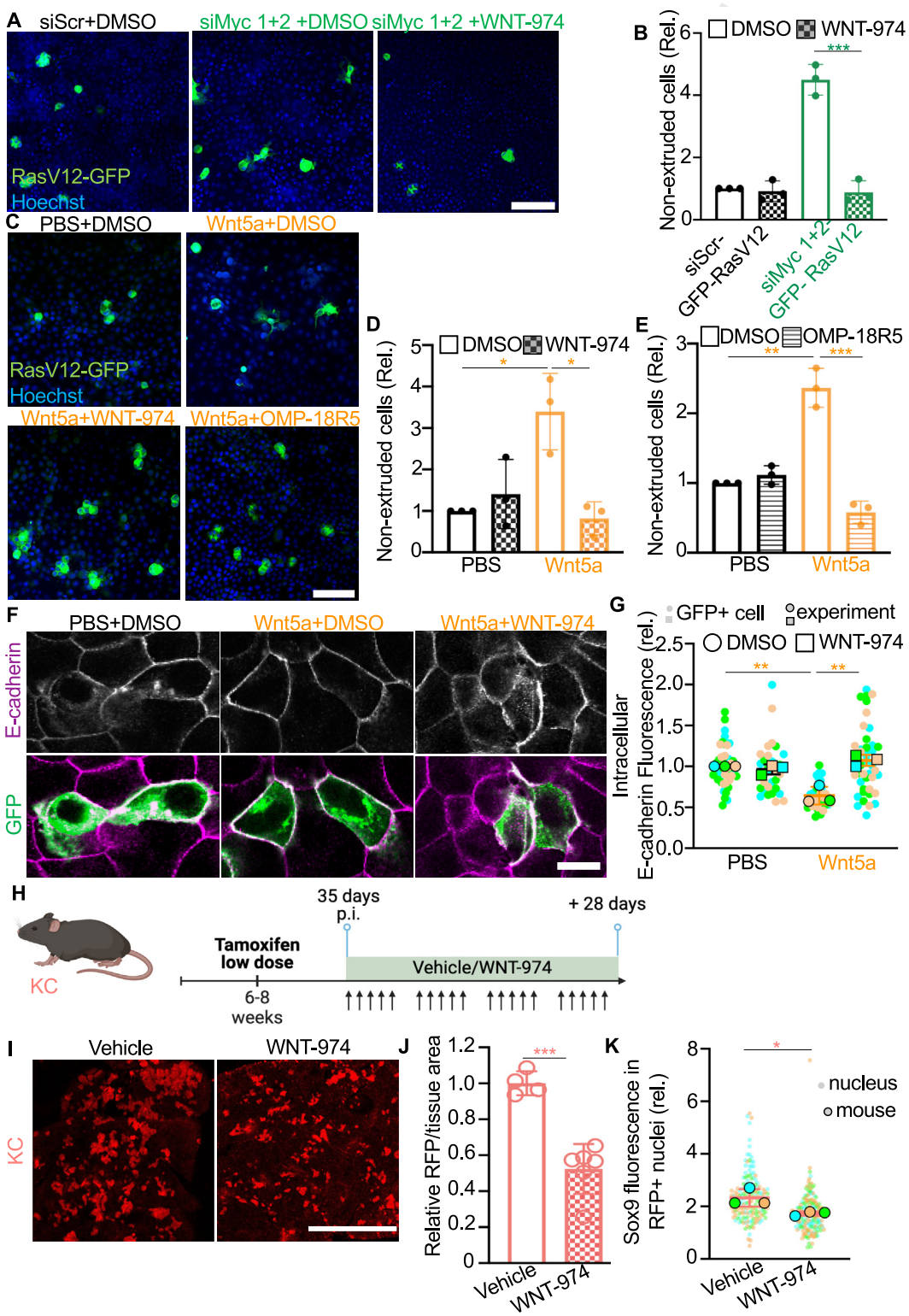

reversed after treatment with WNT-974 (Supplementary Figure 8*G* and *H*).

To functionally test whether active Wnt signaling is necessary for mutant cell retention in vivo, we first induced low-level recombination in adult KC or PC tissues, waited for 35 days p.i. for most mutant cells to be eliminated, and then administered WNT-974 or vehicle for 4 weeks (Figure 6*H*). CD44 fluorescence significantly decreased in WNT-974–treated KC tissues compared with vehicle (Supplementary Figure 9*A*), suggesting Wnt activity is reduced after treatment. We measured a significant decrease in RFP fluorescence in the WNT-974–treated KC tissues (Figure 6*J*–*I*) and in PC tissues (Supplementary Figure 9*B* and *C*) compared to vehicle-treated controls. Thus, inhibition of Wnt pathway induces the expulsion of KrasG12D or p53R172H cells from pancreas tissues in vivo, suggesting Wnt signaling is required to promote mutant cell retention. Notably, we observed a significant decrease in Sox9 fluorescence in RFP^+ nuclei (Figure 6*K*) and a significant decrease in percentage of p27-positive cells (Supplementary Figure 9*D*) in KC tissues treated with WNT-974, compared to KC tissues treated with vehicle. These data suggest that active Wnt signaling is required to promote cell dormancy/cell stemness in some KrasG12D cells in vivo. Our data support a model (Supplementary Figure 9*E*) whereby activation of Wnt signaling allows mutant cells to switch to a dormant cell state, avoid cell expulsion, and survive in the pancreas.

High WNT5A *Expression Correlates With Pancreatic Cancer Progression and Poor Prognosis in Humans*

To translate our findings to the clinical setting, we mined publicly available RNA sequencing[45] and proteomic datasets (Clinical Proteomic Tumour Analysis Consortium, The Cancer Genome Atlas Program). *WNT5A* (Figure 7*A*), *DVL2* (Supplementary Figure 10*A*), *FRIZZLED7* (FZD7, Supplementary Figure 10*B*) gene expression levels were elevated in PanIN lesions and increased pancreatic tumors compared to normal tissues. Expression of WNT5A protein was significantly increased in tumors of increasing grade compared to normal tissues (Figure 7*B*, Supplementary Figure 10*C*). High expression of *WNT5A* correlated with poor overall survival compared to medium/low expression (Figure 7*C*, $P = .1$). FZD7 (Supplementary Figure 10*D*) significantly increased at the protein level in human pancreatic adenocarcinoma samples compared to normal tissues. We conclude that elevated expression of *WNT5A* and high WNT5A signaling are strongly associated with human pancreatic cancer.

Discussion

Tissue homeostasis is fundamental to healthy aging of an organism and cell competition is an important regulator of tissue health. Here, we extend our previously published results[7] to show that, like KrasG12D-expressing cells, p53R172H-expressing cells compete with normal cells for survival in the adult pancreas and are often expelled from the tissue. We report that cell expulsion is inefficient, and a proportion of KrasG12D- or p53R172H-expressing cells are not eliminated from the tissue, suggesting these cells have a survival advantage. We found that Wnt5a signaling is active in noneliminated cells and directly inhibits cell elimination mechanisms both in vitro and in vivo, promoting mutant cell survival. We found that coexpression of p53R172H and KrasG12D in the same cell (KPC) provides all mutant cells with a survival advantage and "double-mutant" KPC cells are not eliminated, consistent with previous studies.[32,46]

Apical cell extrusion is an active process that requires direct interaction with normal cells.[9] E-cadherin is a key modulator of apical cell extrusion,[7,9,40,41] suggesting E-cadherin must be dynamically remodeled for cell extrusion to occur. We previously showed that E-cadherin is decreased at KrasG12D–normal cell–cell adhesions in vivo, specifically at time points before KrasG12D cell elimination,[7] and is predominantly intracellular in KrasG12D-expressing ductal epithelial cells surrounded by normal ductal epithelial cells in vitro.[7] Here, we extended these findings to show that E-cadherin and β-catenin are increased specifically at cell–cell contacts between KrasG12D cells that are not eliminated and normal neighbors in vivo. Using MDCK and primary pancreatic ductal epithelial cell systems, we showed that treatment with Wnt5a induced a significant decrease in the level of intracellular E-cadherin detected in RAS cells. Instead, E-cadherin and β-catenin are increased at RAS–normal cell–cell contacts. Moreover, inhibition of Wnt signaling restores appearance of intracellular E-cadherin in RAS cells and apical extrusion events. Together our data support a model whereby stable cell–cell adhesion induced by Wnt5a signaling prevents cell extrusion. We also found that caveolin-1, an important driver of RasV12 cell

Figure 6. Wnt signaling prevents apical extrusion of RasV12 cells from normal epithelial monolayer in vitro. Inhibition of Wnt promotes elimination of noneliminated cells in vivo. (*A*, *C*) Confocal images of cell extrusion experiment, GFP-RasV12 transfected with siMyc/siScr (*A*) or treated with PBS/Wnt5a (*C*) and DMSO/WNT-974 for 48 hours. *Scale bar:* 100 μm. (*B*) Proportion of nonextruded GFP-RasV12 transfected in (*A*) relative to siScr-GFP-RasV12 (n = 3 experiments). (*D*, *E*) Proportion of GFP-RasV12 nonextruded cells treated with DMSO/WNT-974 (*D*) or DMSO/OMP-18R5 (*E*) relative to PBS-/DMSO-treated cells. (*F*) Confocal *images* of GFP-RasV12 cells mixed with MDCK cells treated with PBS/Wnt5a and DMSO/WNT-974 for 16 hours. *Scale bar:* 20 μm. (*G*) Mean fluorescence intensity of intracellular E-cadherin in GFP-RasV12 in F relative to PBS-/DMSO-treated cells (n = 3 experiments). (*H*) Experimental design for Wnt inhibition experiments in vivo. (*C*) Representative *images* of endogenous RFP fluorescence in KC pancreas harvested 28 days post-vehicle/WNT-974-treatment. *Scale bar:* 500 μm. (*J*) RFP^+ area per total tissue area relative to vehicle (vehicle n = 4 mice; WNT-974 n = 5 mice). (*K*) Mean fluorescence intensity relative to background of Sox9 per nuclei of RFP^+ cells in tissues treated with vehicle/WNT-974 (n = 3 mice). Data represent mean ± SD. Student *t* tests were used to analyze the data. $^*P < .05$; $^{**}P < .001$; $^{***}P < .0001$.

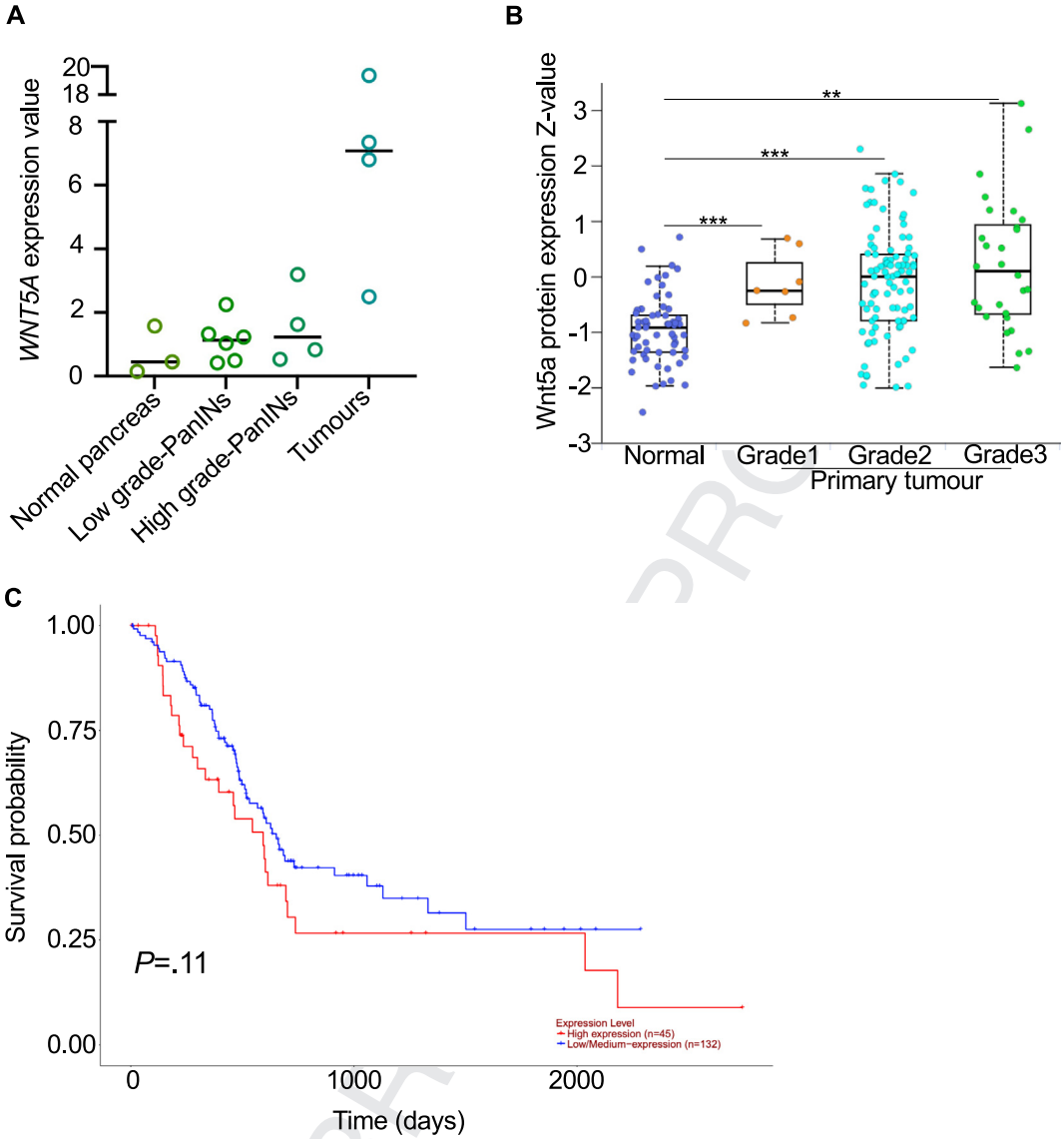

Figure 7. WNT5A protein levels are increased in human pancreatic adenocarcinoma compared to normal human pancreas. (*A*) *WNT5A* expression levels in normal pancreas, low-grade PanINs, high-grade PanINs and tumors (GSE210351). (*B*) The *z* value of WNT5A protein in normal pancreas and pancreatic adenocarcinoma. (*C*) Kaplan-Meier *graph* showing probability of survival depending on high or low *WNT5A* expression levels. $^{**}P < .001$; $^{***}P < .0001$.

extrusion,[42,47] is also decreased at RasV12–normal cell–cell contacts after Wnt5a treatment. In development, Wnt5a signaling regulates cell cohesion and tissue fluidity via caveolin-dependent and clathrin-dependent endocytosis.[48] In human epithelial cells, Wnt5a induces β-catenin membrane localization and association with E-cadherin, increasing intercellular adhesion.[49] Whether Wnt5a directly modulates E-cadherin endocytosis/recycling and/or stability of E-cadherin at the membrane at RasV12–normal cell–cell boundaries requires further investigation.

RasV12 cells in a cell cycle arrested state were not extruded from MDCK monolayers. In pancreas, noneliminated KrasG12D cells stained positive for p27, and upregulated cell dormancy signatures and pathways known to induce cell dormancy.[50] Thus, exiting the cell cycle protects KrasG12D cells from cell elimination in vivo and in vitro. Increased glycolysis and oxidative phosphorylation are also associated with pancreatic cancer stem cells.[51,52] Indeed, our data indicate that some noneliminated KrasG12D cells adopt progenitor and/or stem cell characteristics, suggesting dormant cells are also stem-like cells and may represent a cancer cell of origin. Future studies are required to determine whether normal–mutant interactions in the adult pancreas induce cellular stress responses in genetically mutant cells and whether this in turn activates cell dormancy. Interestingly, Wnt5a has been shown to induce and maintain cancer cell dormancy in metastatic niches by negatively regulating canonical Wnt/β-catenin signaling.[34,35] An exciting future direction of this work will be to elucidate whether the cell dormancy phenotype described here is regulated via Wnt-dependent mechanisms described for dormant metastatic cancer cells. Here, we

show that inhibition of Wnt restores cell extrusion and cell segregation of cell cycle arrested RasV12 cells from normal cells in vitro. Sox9 levels in RFP^+ nuclei significantly decreased and percentage of p27-positive KrasG12D cells are significantly reduced in WNT-974–treated tissues, suggesting a mechanistic link between active Wnt and cell dormancy/cell stemness in vivo is plausible.

KRAS is a key driver of pancreatic ductal adenocarcinoma. Single-cell profiling of pancreatic tumorigenesis in mouse models demonstrates that *Kras* mutant cells are very heterogeneous and show signatures of tumorigenesis even before premalignant lesions are established.[20] Our RNA sequencing data confirmed this early transformation and cellular heterogeneity profile of KrasG12D cells. Pancreatic cancer is a devastating disease, which is generally diagnosed at late and incurable stages. An improved understanding of the biology of how pancreatic cancer starts and grows in adult tissues will inform the development of new early-detection tools. Our results challenge current understanding of how cancers start in the adult pancreas and suggest that genetically mutant cells must override tissue homoeostasis mechanisms to survive in tissues, before malignant transformation/expansion.

Supplementary Material

Q18 Note: To access the supplementary material accompanying this article, visit the online version of *Gastroenterology* at www.gastrojournal.org, and at https://doi.org/10.1053/j.gastro.2025.02.042.

References

1. van Neerven SM, Vermeulen L. Cell competition in development, homeostasis and cancer. Nat Rev Mol Cell Biol 2023;24:221–236.
2. Sasaki A, Nagatake T, Egami R, et al. Obesity suppresses cell-competition-mediated apical elimination of RasV12-transformed cells from epithelial tissues. Cell Rep 2018;23:974–982.
3. Fernandez-Antoran D, Piedrafita G, Murai K, et al. Outcompeting p53-mutant cells in the normal esophagus by redox manipulation. Cell Stem Cell 2019;25:329–341.e6.
4. Alcolea MP, Greulich P, Wabik A, et al. Differentiation imbalance in single oesophageal progenitor cells causes clonal immortalization and field change. Nat Cell Biol 2014;16:615–622.
5. Flanagan DJ, Pentinmikko N, Luopajarvi K, et al. NOTUM from Apc-mutant cells biases clonal competition to initiate cancer. Nature 2021;594:430–435.
6. van Neerven SM, de Groot NE, Nijman LE, et al. Apc-mutant cells act as supercompetitors in intestinal tumour initiation. Nature 2021;594:436–441.
7. Hill W, Zaragkoulias A, Salvador-Barbero B, et al. EPHA2-dependent outcompetition of KRASG12D mutant cells by wild-type neighbors in the adult pancreas. Curr Biol 2021;31:2550–2560.e5.
8. Hill W, Hogan C. Normal epithelial cells trigger EphA2-dependent RasV12 cell repulsion at the single cell level. Small GTPases 2019;10:305–310.
9. Hogan C, Dupre-Crochet S, Norman M, et al. Characterization of the interface between normal and transformed epithelial cells. Nat Cell Biol 2009;11:460–467.
10. Porazinski S, de Navascues J, Yako Y, et al. EphA2 drives the segregation of Ras-transformed epithelial cells from normal neighbors. Curr Biol 2016;26:3220–3229.
11. Lanfredini S, Thapa A, O'Neill E. RAS in pancreatic cancer. Biochem Soc Trans 2019;47:961–972.
12. Collins MA, Bednar F, Zhang Y, et al. Oncogenic Kras is required for both the initiation and maintenance of pancreatic cancer in mice. J Clin Invest 2012;122:639–653.
13. Bailey P, Chang DK, Nones K, et al. Genomic analyses identify molecular subtypes of pancreatic cancer. Nature 2016;531:47–52.
14. Morton JP, Timpson P, Karim SA, et al. Mutant p53 drives metastasis and overcomes growth arrest/senescence in pancreatic cancer. Proc Natl Acad Sci U S A 2010;107:246–251.
15. Jackson EL, Willis N, Mercer K, et al. Analysis of lung tumor initiation and progression using conditional expression of oncogenic K-ras. Genes Dev 2001;15:3243–3248.
16. Olive KP, Tuveson DA, Ruhe ZC, et al. Mutant p53 gain of function in two mouse models of Li-Fraumeni syndrome. Cell 2004;119:847–860.
17. Luche H, Weber O, Nageswara Rao T, et al. Faithful activation of an extra-bright red fluorescent protein in "knock-in" Cre-reporter mice ideally suited for lineage tracing studies. Eur J Immunol 2007;37:43–53.
18. Parfitt GJ. Immunofluorescence tomography: high-resolution 3-D reconstruction by serial-sectioning of methacrylate embedded tissues and alignment of 2-D immunofluorescence images. Sci Rep 2019;9:1992.
19. Woolley TE, Hill W, Hogan C. Accounting for dimensional differences in stochastic domain invasion with applications to precancerous cell removal. J Theor Biol 2022;541:111024.
20. Burdziak C, Alonso-Curbelo D, Walle T, et al. Epigenetic plasticity cooperates with cell-cell interactions to direct pancreatic tumorigenesis. Science 2023;380:eadd5327.
21. Ma Z, Lytle NK, Chen B, et al. Single-cell transcriptomics reveals a conserved metaplasia program in pancreatic injury. Gastroenterology 2022;162:604–620.e20.
22. Kim RS, Avivar-Valderas A, Estrada Y, et al. Dormancy signatures and metastasis in estrogen receptor positive and negative breast cancer. PLoS One 2012;7:e35569.
23. Jiang Z, Wu F, Laise P, et al. Tff2 defines transit-amplifying pancreatic acinar progenitors that lack regenerative potential and are protective against Kras-driven carcinogenesis. Cell Stem Cell 2023;30:1091–1109.e7.
24. Benn J, Schneider RJ. Hepatitis B virus HBx protein deregulates cell cycle checkpoint controls. Proc Natl Acad Sci U S A 1995;92:11215–11219.

25. Toyoshima H, Hunter T. p27, a novel inhibitor of G1 cyclin-Cdk protein kinase activity, is related to p21. Cell 1994;78:67–74.
26. Payne KK. Cellular stress responses and metabolic reprogramming in cancer progression and dormancy. Semin Cancer Biol 2022;78:45–48.
27. Hussein AM, Balachandar N, Mathieu J, et al. Molecular regulators of embryonic diapause and cancer diapause-like state. Cells 2022;11:2929.
28. Fox DB, Garcia NMG, McKinney BJ, et al. NRF2 activation promotes the recurrence of dormant tumour cells through regulation of redox and nucleotide metabolism. Nat Metab 2020;2:318–334.
29. Easwaran S, Van Ligten M, Kui M, et al. Enhanced germline stem cell longevity in *Drosophila* diapause. Nat Commun 2022;13:711.
30. Itahana K, Dimri GP, Hara E, et al. A role for p53 in maintaining and establishing the quiescence growth arrest in human cells. J Biol Chem 2002;277:18206–18214.
31. Wiecek AJ, Cutty SJ, Kornai D, et al. Genomic hallmarks and therapeutic implications of G0 cell cycle arrest in cancer. Genome Biol 2023;24:128.
32. Watanabe H, Ishibashi K, Mano H, et al. Mutant p53-expressing cells undergo necroptosis via cell competition with the neighboring normal epithelial cells. Cell Rep 2018;23:3721–3729.
33. Scognamiglio R, Cabezas-Wallscheid N, Thier MC, et al. Myc depletion induces a pluripotent dormant state mimicking diapause. Cell 2016;164:668–680.
34. Fane ME, Chhabra Y, Alicea GM, et al. Stromal changes in the aged lung induce an emergence from melanoma dormancy. Nature 2022;606:396–405.
35. Ren D, Dai Y, Yang Q, et al. Wnt5a induces and maintains prostate cancer cells dormancy in bone. J Exp Med 2019;216:428–449.
36. van der Weijden VA, Bulut-Karslioglu A. Molecular regulation of paused pluripotency in early mammalian embryos and stem cells. Front Cell Dev Biol 2021;9:708318.
37. Flanagan DJ, Phesse TJ, Barker N, et al. Frizzled7 functions as a Wnt receptor in intestinal epithelial Lgr5(+) stem cells. Stem Cell Reports 2015;4:759–767.
38. Abedini A, Sayed C, Carter LE, et al. Non-canonical WNT5a regulates epithelial-to-mesenchymal transition in the mouse ovarian surface epithelium. Sci Rep 2020;10:9695.
39. Wielenga VJ, Smits R, Korinek V, et al. Expression of CD44 in Apc and Tcf mutant mice implies regulation by the WNT pathway. Am J Pathol 1999;154:515–523.
40. Grieve AG, Rabouille C. Extracellular cleavage of E-cadherin promotes epithelial cell extrusion. J Cell Sci 2014;127:3331–3346.
41. Saitoh S, Maruyama T, Yako Y, et al. Rab5-regulated endocytosis plays a crucial role in apical extrusion of transformed cells. Proc Natl Acad Sci U S A 2017;114:E2327–E2336.
42. Ohoka A, Kajita M, Ikenouchi J, et al. EPLIN is a crucial regulator for extrusion of RasV12-transformed cells. J Cell Sci 2015;128:781–789.
43. Lin HK, Lin HH, Chiou YW, et al. Caveolin-1 downregulation is required for Wnt5a-Frizzled 2 signalling in Ha-Ras(V12) -induced cell transformation. J Cell Mol Med 2018;22:2631–2643.
44. Flanagan DJ, Woodcock SA, Phillips C, et al. Targeting ligand-dependent wnt pathway dysregulation in gastrointestinal cancers through porcupine inhibition. Pharmacol Ther 2022;238:108179.
45. Liffers ST, Godfrey L, Frohn L, et al. Molecular heterogeneity and commonalities in pancreatic cancer precursors with gastric and intestinal phenotype. Gut 2023;72:522–534.
46. Haraoka Y, Akieda Y, Nagai Y, et al. Zebrafish imaging reveals TP53 mutation switching oncogene-induced senescence from suppressor to driver in primary tumorigenesis. Nat Commun 2022;13:1417.
47. Teo JL, Gomez GA, Weeratunga S, et al. Caveolae control contractile tension for epithelia to eliminate tumor cells. Dev Cell 2020;54:75–91.e7.
48. Puzik K, Tonnier V, Opper I, et al. Lef1 regulates caveolin expression and caveolin dependent endocytosis, a process necessary for Wnt5a/Ror2 signaling during Xenopus gastrulation. Sci Rep 2019;9:15645.
49. Medrek C, Landberg G, Andersson T, et al. Wnt-5a-CKIalpha signaling promotes beta-catenin/E-cadherin complex formation and intercellular adhesion in human breast epithelial cells. J Biol Chem 2009;284:10968–10979.
50. Risson E, Nobre AR, Maguer-Satta V, et al. The current paradigm and challenges ahead for the dormancy of disseminated tumor cells. Nat Cancer 2020;1:672–680.
51. Sancho P, Burgos-Ramos E, Tavera A, et al. MYC/PGC-1alpha balance determines the metabolic phenotype and plasticity of pancreatic cancer stem cells. Cell Metab 2015;22:590–605.
52. Valle S, Alcala S, Martin-Hijano L, et al. Exploiting oxidative phosphorylation to promote the stem and immunoevasive properties of pancreatic cancer stem cells. Nat Commun 2020;11:5265.

Received August 28, 2024. Accepted February 23, 2025.

Correspondence
Address correspondence to: Catherine Hogan, PhD, European Cancer Stem Cell Research Institute, School of Biosciences, Cardiff University, Cardiff CF24 4HQ, UK. e-mail: hoganc@cardiff.ac.uk. Q4

Acknowledgments
The authors thank A. Marchbank and colleagues at School of Biosciences Genome Hub (Cardiff University) and Wales Gene Park for technical support with RNA sequencing experiments and A. Gibbs (Wales Cancer Research Centre) for bioinformatics support. The authors thank colleagues at European Cancer Stem Cell Research Institute, School of Biosciences, Cardiff University: T. Phesse and V. Meniel for Wnt antagonists and helpful discussions; F. Afonso for critical reading of the manuscript and helpful discussions. The manuscript was critically reviewed by C. Winchester (Cancer Research UK Scotland Institute).

CrediT Authorship Contributions Q5
Beatriz Salvador-Barbero, PhD (Conceptualization: Equal; Data curation: Lead; Formal analysis: Lead; Funding acquisition: Supporting; Investigation: Lead; Methodology: Lead; Software: Lead; Validation: Lead; Visualization: Lead; Writing – original draft: Supporting; Writing – review & editing: Equal)

Markella Alatsatianos, PhD (Investigation: Supporting; Methodology: Supporting; Validation: Supporting; Writing – review & editing: Supporting)

Jennifer P. Morton, PhD (Funding acquisition: Supporting; Resources: Supporting; Writing – review & editing: Supporting)

Owen J. Sansom, PhD (Funding acquisition: Supporting; Resources: Supporting; Writing – review & editing: Supporting)

Catherine Hogan, PhD (Conceptualization: Lead; Funding acquisition: Lead; Methodology: Supporting; Project administration: Lead; Resources: Lead; Supervision: Lead; Writing – original draft: Lead; Writing – review & editing: Equal)

Conflicts of interest Q6

The authors disclose no conflicts.

Funding

Q7 Q24 Beatriz Salvador-Barbero and Markella Alatsatianos were supported by Cancer Research UK (CRUK) Early Detection project grant (A27838) to Catherine Hogan (lead principal investigator [PI]) and Owen J. Sansom (co-investigator) and Jennifer P. Morton (co-investigator). Owen J. Sansom and Jennifer P. Morton were supported by CRUK core funding to the CRUK Scotland Institute (A17196 and A31287) to Owen J. Sansom laboratory (A21139) and to Jennifer P. Morton laboratory (A29996). Beatriz Salvador-Barbero is currently funded by a Pancreatic Cancer UK Career Foundation Fellowship (176937364). This study was supported by CRUK Early Detection project grant (A27838) to Catherine Hogan. Q8

Data Availability

The RNA-sequencing data generated during this study are available at GEO ID: GSE255283 (https://eur03.safelinks.protection.outlook.com/?url = https%3A%2F%2Fwww.ncbi.nlm.nih.gov%2Fgeo%2Fquery%2Facc.cgi%3Facc%3DGSE255283&data = 05%7C02%7Csalvadorb%40cardiff.ac.uk%7Ce8683ba7b2c64f0a3bce08dc280f1f5c%7Cbdb74b3095684856bdbf06759778fcbc%7C1%7C0%7C638429292617229243%7CUnknown%7CTWFpbGZsb3d8eyJWIjoiMC4wLjAwMDAiLCJQIjoiV2luMzIiLCJBTiI6Ik1haWwiLCJXVCI6Mn0%3D%7C0%7C%7C%7C%7C&sdata = 5jxRazg7lAf2W2wqa%2Bwfa7kxPY9HVX01VXHr4PZQVA0%3D&reserved = 0). Currently, the data are not publicly available; reviewers can access the data using the token krcxkmcihrklhqh. Data will be publicly available when the manuscript is accepted for publication. Q9 Q10

Supplementary Methods

Mouse Lines, Induction of Cre Recombinase In Vivo, Inhibition of Wnt In Vivo

Pdx1-Cre^{ERT}, *LSL-Kras*$^{G12D/+}$, *LSL-Trp53*$^{R172H/+}$, *Rosa26*$^{LSL\text{-}tdRFP}$ mouse lines have all been described previously.[7] Animals were housed in conventional pathogen-free animal facilities and experiments were conducted in accordance with UK Home Office regulations (ASPA 1986 and EU Directive 2010) under the guidelines of Cardiff University Animal Welfare and Ethics Committee. Mice were genotyped by polymerase chain reaction analysis following standard methods and using previously published primer sequences.[7] Both male and female 6- to 8-week-old experimental and control mice were injected with intraperitoneal injection of tamoxifen in corn oil as described previously.[7] Low recombination levels were obtained by administering 1 tamoxifen dose of 1 μg/40 g bodyweight, while high recombination (megadose) was induced by 3 injections of 9 mg/40 g over 5 days.[7] Pancreata were harvested at 7, 35, 70, 140, or 168 days post tamoxifen induction. To test the functional role of Wnt signaling in vivo, 6- to 8-week-old experimental and control mice were induced with low-dose tamoxifen, aged to 35 days post induction of Cre recombinase (p.i.) and treated with WNT-974 1.5 mg/kg or vehicle (DMSO) in corn oil by oral gavage, 5 days per week for 4 weeks. At the end of the treatment pancreatic tissue was harvested and treated as described below. No statistical method was used to predetermine sample size. For most animal studies, experiments were not randomized, and investigators were not blinded to allocation during experiments. To test the functional role of Wnt signaling mice were randomly allocated into vehicle or WNT-974–treated groups. All experiments were reproduced using at least 3 animals of each genotype.

Pancreas Digestion and RNA Sequencing

Pancreas tissues were harvested 35 days post low-dose tamoxifen induction. To reach the minimum of 5000 cells and a minimum of 100 ng RNA/sample for bulk RNA sequencing, we combined 3 pancreas tissues of the same genotype to produce 1 sample per genotype. Each sample was replicated 3 times to generate 3 biological repeats per genotype for sequencing. Pancreas tissues were digested as described previously.[e1] Using an ethylene glycol-bis(β-aminoethyl ether)-*N,N,N′,N′*-tetraacetic acid–based buffer the pancreas from each mouse was inflated and slightly digested with collagenase. The tissue was chopped and further digested using a calcium-based buffer with collagenase. Single-cell digested tissue was stained with leptin PNA-A488 (ThermoFisher) and 4′,6-diamidino-2-phenylindole (ThermoFisher Scientific). 4′,6-Diamidino-2-phenylindole–negative, leptin-positive, RFP-positive cells were sorted using the FACSAria Fusion sorter (BD Biosciences). A minimum of 5000 cells were sorted for each sample. RNA was extracted using the RNeasy Micro kit (Qiagen) following the manufacturer's recommendations. Paired-end sequencing was performed using Sanger sequencing Illumina 1.9. Sequenced reads Fastq files were quality-checked using FastQC. Reads were aligned to the mouse genome (Ensembl-GRCm38 *Mus musculus*) using the STAR package, and reads were counted using the FeatureCounts package, after removing duplicates using the MarkDuplicates tool (GATK). Differential expression was normalized and calculated using DESeq2, comparing the different genotypes against the control. Finally, GSEA software, version 4.2.2 was used for enrichment analysis of different pathways and Prism software, version 10.0.2 (GraphPad) for heatmap graphs and normalized enrichment score graphs. The RNA sequencing data generated during this study are available at GEO ID: GSE255283 (reviewers token krcxkmcihrklhqh).

Madin-Darby Canine Kidney Cell Lines and In Vitro Experiments

To assess the interactions between RasV12 and MDCK cells, MDCK-pTR GFP–RasV12 cells were combined with parental MDCK cells at a 1:50 ratio.[9,10] Treatment with tetracycline (2 μg/mL) induces GFP-RasV12 expression in MDCK-pTR GFP–RasV12 cells.[9,10] Cells were plated at a density of 2.5×10^5 cells per well in MW24 plates (Corning) carrying 18-mm diameter glass cover slips (VWR). Mixed cells were incubated for 30 hours or 48 hours at 37°C before fixed with 4% formaldehyde (ThermoFisher Scientific). Cells were then permeabilized and stained (Supplementary Table 14). GFP-RasV12 cells were considered nonextruded when >30% of their cytoplasm was basally protruded. Three technical replicates per experiment in 3 experiments (ie, using 3 independent passages from at least 2 frozen stocks of parental and GFP-RasV12 MDCK cells) were performed and at least 150 GFP-RasV12 cells were quantified per replicate.

For c-Myc silencing, tetracyclin-induced GFP-RasV12 cells were transfected with 100 ng siRNA oligos targeting *Myc* using Lipofectamine 3000 (Invitrogen) (siRNA siMyc1: AAGACGUUGUGUGUUCGCCUC – as GAGGCGAACACACAACGUCUU, siRNA siMyc2: AAUUUCAACUGUUCUCGCCGC – as GCGGCGAGAACAGUUGAAAUU and siScr). For cell extrusion and proliferation experiments, GFP-RasV12 cells were trypsinized and mixed with parental MDCK cells 24 hours after siMyc1+2 transfection and were then fixed following a further 48 hours.

For experiments comparing PBS, Wnt3a, and Wnt5a treatments effect, RasV12 cells were mixed 1:50 with parental MDCK cells and once cells were set, induced with tetracycline. Two hours post-tetracycline induction, cells were treated with 1 μg/mL of human recombinant Wnt3a (Peprotech), 100 ng/mL of human recombinant human/mouse Wnt5a (R&D Systems), or PBS (control-Sigma-Aldrich). Cells were fixed 30 hours after PBS, Wnt3a, or Wnt5a treatment for cell extrusion analysis and for analysis of E-cadherin/β-catenin at the RasV12-MDCK contact or within GFP-RasV12 cell clusters. E-cadherin endocytosis and caveolin fluorescence were assessed by fixing cells 16 hours after PBS/Wnt5a treatment.

For Wnt pathway inhibition experiments, tetracycline induced GFP-RasV12 cells were transfected with siMyc1+2/siScr or treated with recombinant Wnt5a/PBS for 24 hours and then mixed with parental MDCK cells. Wnt5a treatment was maintained during the whole experiment. WNT-974 (Stratech) porcupine inhibitor (1 μM) or *OMP*-18R5 (10 mg/mL) was added to the medium 8 hours after GFP-RasV12 and MDCK cells were mixed and plated. DMSO-treated GFP-RasV12 cells were used as control for both inhibitors. To assess cell extrusion, cells were fixed 48 hours after plating. E-cadherin endocytosis was assessed by mixing RasV12 cells with MDCK parental cells, then RasV12 expression was induced by tetracycline and treated with PBS or Wnt5a 2 hours after. Four hours after PBS/Wnt5a treatment, cells were treated with DMSO or WNT-974. Cells were fixed 16 hours after PBS/Wnt5a treatment.

Immunofluorescent staining was performed by permeabilization of cells with 0.05% SDS (Sigma-Aldrich) and 0.05% Triton X100 (Sigma-Aldrich) solution for 15 minutes. Cells were stained with anti–Ki-67, anti–E-cadherin, anti–β-catenin or Caveolin primary antibodies for 2 hours at room temperature, Alexa Fluor secondary antibody incubation for 60 minutes at room temperature and Hoechst (ThermoFisher) (Supplementary Table 14) and mounted using Mowiol (Sigma-Aldrich). For proliferation analysis at least 30 extruded and 30 nonextruded cells were quantified in siMyc 1+2 treated cells per experimental replicate (ie, using 3 independent passages of parental and GFP-RasV12 MDCK cells). For E-cadherin, β-catenin, or Caveolin at least 10 GFP-RasV12 cell clusters per experimental replicate were quantified. Fluorescence intensity at the border between RasV12 and parental MDCK cells were quantified by measuring mean fluorescence intensity of 2.27 $\times$ 2.27-pixel circles (regions of interest) along the membrane separated by approximately 5 pixels. E-cadherin endocytosis was measured quantifying the mean fluorescence intensity of the cytoplasm of each RasV12 cell. At least 10 cells were quantified in 3 technical replicates per experiment in 3 experiments.

Confrontation assays and migration speed analysis were carried out as described.[10] The 1 $\times$ 10^4 cells were plated in inserts (Ibidi) in MW24 plates, allowed to form monolayers (8 hours) before removing the insert and moving the plate to IncuCyte S3 (Sartorius) for live cell imaging. Images were captured every 15 minutes for 48 hours. siMyc/siScr-GFP-RasV12 cells were plated 24 hours after transfection and inserts were removed 8 hours post transfection. For Wnt5a experiments, cells were treated with PBS/Wnt5a for 8 hours before inserts were removed. PBS/Wnt5a treatment was maintained during the whole experiment. WNT-974 porcupine inhibitor (Stratech)/DMSO (Sigma-Aldrich) was added to the medium when inserts were removed. Retraction was measured as the distance GFP-RasV12 cells migrated during 24 hours, following initial cell–cell collision with MDCK cells. Coefficient of boundary smoothness was measured using Fiji in cell confrontation assays at the end of the 24-hour experiment and as described previously.[10] This was calculated by measuring the length of the cell–cell boundary between GFP-RasV12 and MDCK cells at the end of the experiment (*dashed line* in Supplementary Figure 8*A*) divided by the length of a straight line from the top to the bottom of the collision (*solid line* in Supplementary Figure 8*A*). A value of 1.0 indicates a linear boundary. We performed 3 technical replicates per experiment in 3 experiments (ie, using 3 independent passages of parental and GFP-RasV12 MDCK cells).

Western blotting was performed using GFP-RasV12 cell lysates transfected with siMyc/siScr siRNAs at 48 hours post transfection (Supplementary Figure 3*E*), treated for 48 hours with WNT-974/DMSO 24 hours post transfection (Supplementary Figure 5*D*). Cells were lysed using Laemmli buffer (0.0625 M Tris base, 2% sodium dodecyl sulfate, 10% glycerol). Proteins were separated on 12% polyacrylamide gels under reducing polyacrylamide gel electrophoresis conditions. Proteins were then transferred to polyvinylidene difluoride membranes (Immobilon-P, Merck) using wet transfer (1 hour, 100 V). Membranes were blocked in 5% milk Tris-buffered saline with Tween 20 for 1 hour and antibodies were added in the same buffer at the concentrations listed in Supplementary Table 14 for overnight at 4°C or 2 hours at room temperature. Secondary antibodies (Supplementary Table 14) were added in 5% milk Tris-buffered saline with Tween 20 and membranes were developed using ECL luminol kit (Merck) and chemiluminescence films (Amersham Hyperfilm ECL, GE Healthcare). Protein levels were quantified using Fiji (RRID:SCR_002285) software "Gels" tool.

Real-time cell confluency was measured using Incucyte S3 live cell imaging instrument and software (version 2020). The 1 $\times$ 10^3 cells siMyc/siScr-GFP-RasV12 cells were plated 24 hours after transfection with siMyc/siScr siRNAs in MW96 (Corning). Images were captured every 15 minutes for 48 hours. We performed 3 technical replicates per experiment in 3 experiments.

Imaging and Image Analysis

Immunohistochemical imaging was done using the Axio Scan Z1 slide scanner (Zeiss) 20$\times$ magnification. Fluorescence imaging of tissue sections was carried out a Zeiss LSM710 confocal microscope. Fluorescence imaging of MDCK/PDEC cell cultures was performed using Zeiss LSM880 or Leica Sp8 confocal microscope.

The percentage of RFP^+ tissue area was determined using endogenous RFP levels quantified as described.[7] Using Fiji (RRID:SCR_002285) software, positive areas were thresholded using RFP fluorescence. Tissue autofluorescence was used to determine total tissue area. The percentage of RFP^+ ducts were analyzed using E-cadherin/RFP/Hoechst-stained sections to identify ducts. At least 20 ducts were quantified per mouse and ducts were considered positive when they contained at least 1 RFP^+ cell. The percentage of RFP^+ cells in pancreatic islets were scored in FFPE immunohistochemical sections stained with anti-RFP antibody and using "positive cell count" tool in QuPath-0.4.1 software. RFP^+ cluster size, perimeter, and area were determined in FFPE immunohistochemical sections stained with anti-RFP antibody and using QuPath software, version 0.4.1 by analyzing shape features of RFP^+ (3,3′-diaminobenzidine tetra hydrochloride–positive) areas. Ki-

67–positive and cleaved caspase-3–positive cells were analyzed using QuPath software, version 0.4.1 positive cell count feature.

Wnt5a fluorescence intensity in the tissue was quantified by masking the tissue area (AF568) and measuring mean fluorescence intensity for Wnt5a (AF488). CD44, β-catenin, and E-cadherin fluorescence intensity at the border between RFP-positive and -negative cells were quantified by measuring mean fluorescence intensity of 2.43 × 2.43-pixel circles (regions of interest) along the membrane (RFP^+/RFP^-) separated by approximately 5 pixels. CD44, Dvl2, and K-cadherin fluorescence in clusters was quantified by masking RFP^+ (AF568) areas and quantifying mean fluorescence intensity for CD44/Dvl2/K-cadherin (AF488). β-catenin and Sox9 fluorescence in nuclei was quantified by masking nuclei (Hoechst) and quantifying mean fluorescence intensity for β-catenin/Sox9 (AF488) in RFP^+ cells. To avoid noise associated with tissue autofluorescence, fluorescence intensity measurements were made relative to image global mean fluorescence intensity (AF488).

Children's Brain Tumor Network, The Cancer Genome Atlas, and GSE210351 Data Analysis

Children's Brain Tumor Network and The Cancer Genome Atlas data were analyzed using UALCAN data analysis portal. The z values represent SDs from the median across samples for the given cancer type. Log2 spectral count ratio values from Clinical Proteomic Tumour Analysis Consortium were first normalized within each sample profile, then normalized across samples. GSE210351 data[45] were analyzed using Geo2R-GEO-NCBI tool.

Statistical Tests

Statistical analyses were performed using Prism 10 software (GraphPad). Normally distributed data, as determined by the Shapiro-Wilke test or D'Agostino and Pearson test were analyzed using unpaired Student t tests. Human data statistical analysis was performed using the UALCAN data analysis portal. A P value of $<.05$ was considered as significant and a rejection of the null hypothesis. Graphical data represent mean ± SD. No statistical method was used to predetermine sample size. Definition of n is in the figures. GSEA was performed using GSEA software, version 4.2.2. GSEA was used to identify gene sets that were differentially expressed between 2 groups of samples. Gene sets were considered enriched if they had a false discovery rate of <0.25. Heatmaps were created by computing normalized gene counts for each individual sample into row z scores. SuperPlots show all the quantified points (smaller circles) and the mean for each mouse/experiment (larger circles).

Supplementary References

e1. Assi M, Dauguet N, Jacquemin P. DIE-RNA: a reproducible strategy for the digestion of normal and injured pancreas, isolation of pancreatic cells from genetically engineered mouse models and extraction of high quality RNA. Front Physiol 2018;9:129.

e2. Dudgeon C, Harris CR, Chen Y, et al. A novel model of pancreatic cancer dormancy reveals mechanistic insights and a dormancy gene signature with human relevance. 2020. bioRxiv 2020;04.13:037374.

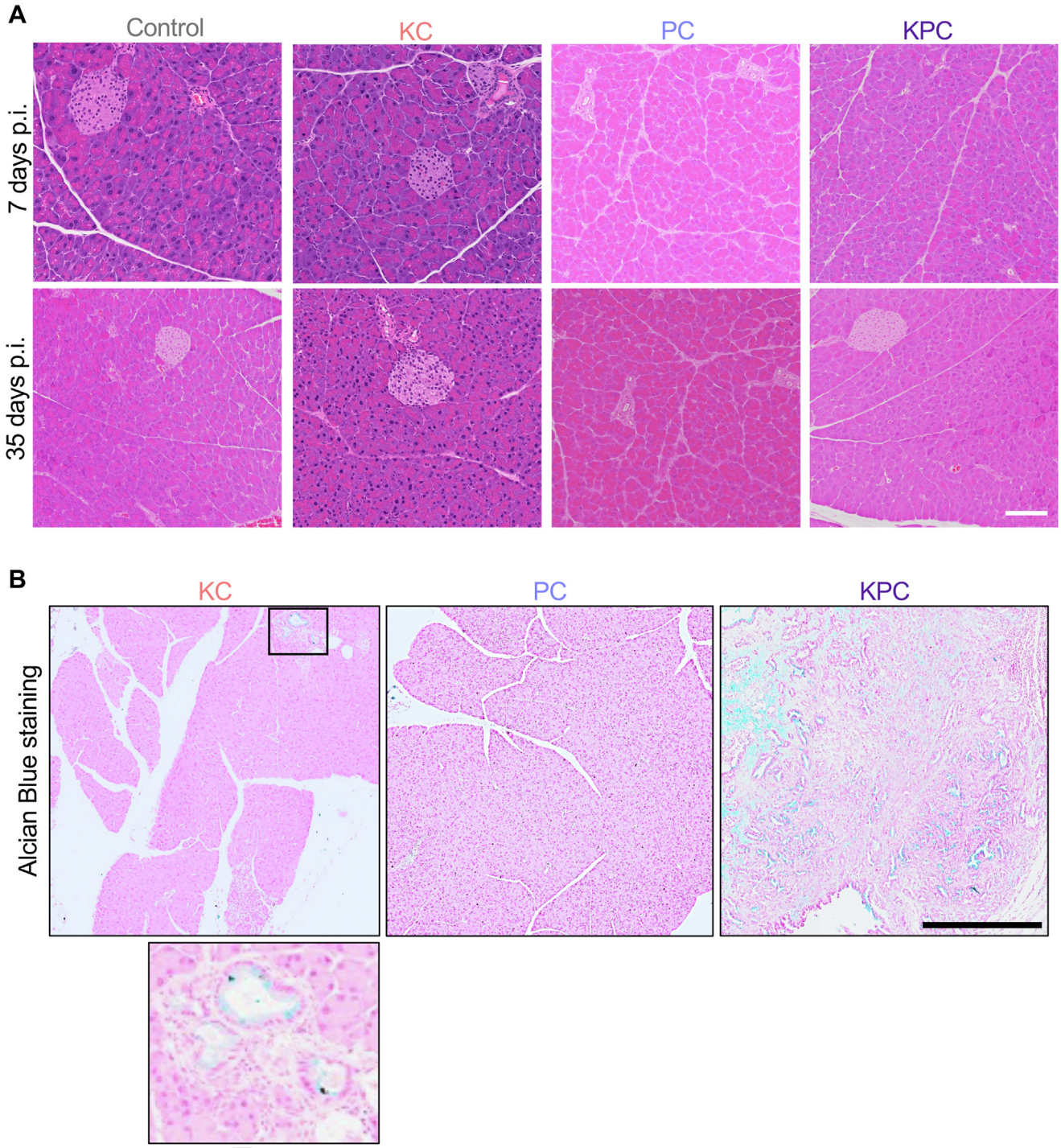

Supplementary Figure 1. Noneliminated mutant cells can progress to mucin-positive lesions. (*A*) H&E staining of pancreas tissues harvested at 35 days p.i. from control, KrasG12D (KC), p53R172H (PC) or double mutant (KPC) expressing mice. *Scale bar:* 100 μm. (*B*) Pancreas tissues from KC, PC, and KPC mice harvested at 168 days p.i. and stained for mucin (using Alcian blue). *Scale bar:* 500 μm. *Boxed area* shown magnified (*lower panel*).

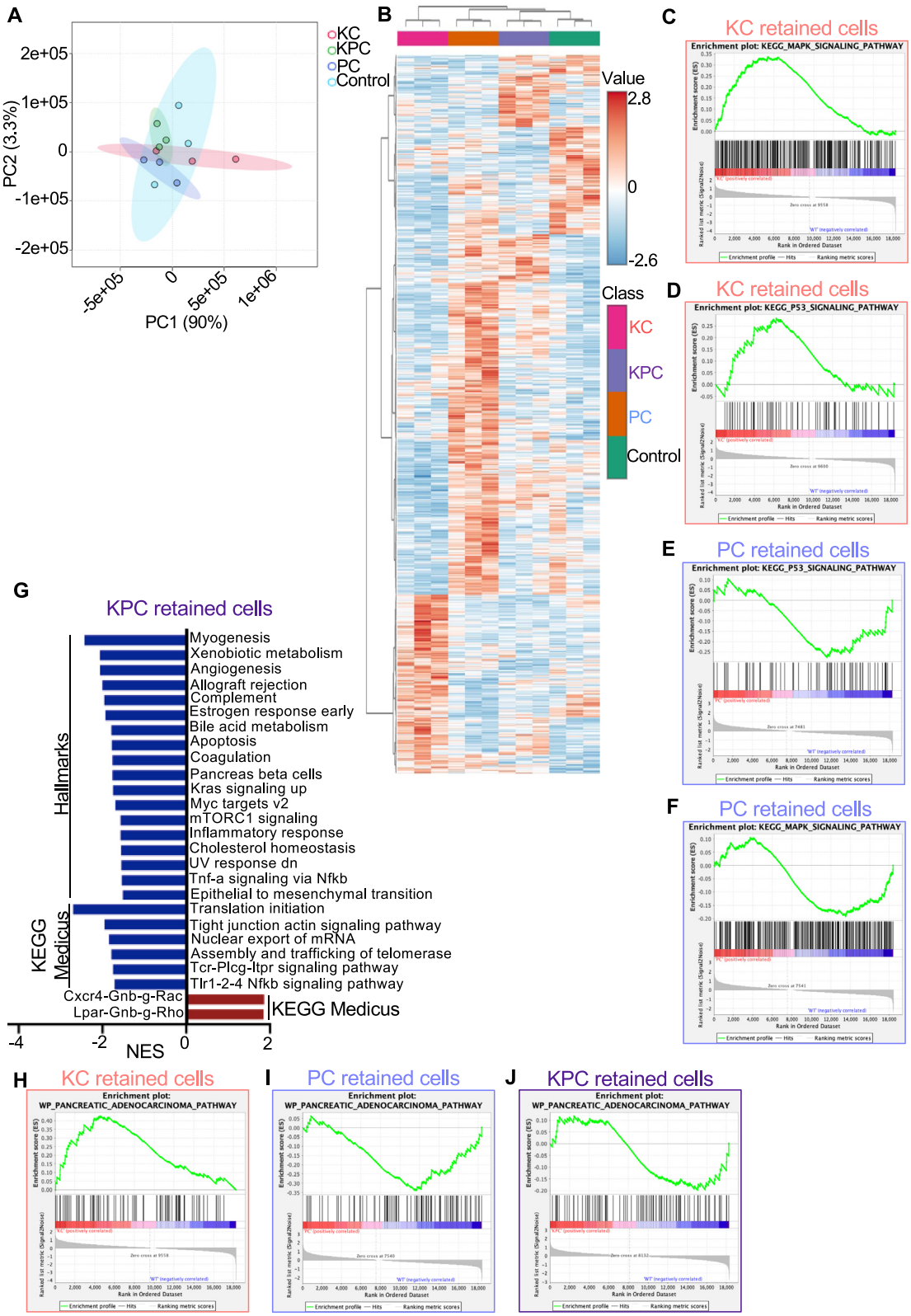

print & web 4C/FPO

Supplementary Figure 2. Transcriptomic analysis indicates Kras and p53 pathways deregulation in retained cells. (*A*) Principal component analysis of control, KrasG12D (KC), p53R172H (PC) or double-mutant (KPC) transcriptomic data obtained at 35 days p.i. PC1 and PC2 of normalized data are shown. (*B*) Unsupervised clustering heatmap of the top 2500 differentially expressed genes (after normalization) between the 12 samples sequenced (3× Control, KC, PC and KPC). GSEA enrichment plots showing (*C*) KEGG_MAPK_signaling_pathway (M10792) and (*D*) KEGG_p53_signaling_pathway (M6370) positive correlation in KC cells compared to control and (*E*) KEGG_p53_signaling_pathway (M6370), and (*F*) KEGG_MAPK_signaling_pathway (M10792) negative correlation in PC cells compared to control. (*G*) Normalized enrichment scores (NES) of GSEA on the Hallmarks and KEGG Medicus gene sets for the RNA sequencing experiment analysis of KPC retained cells. Only gene sets with an false discovery rate of <0.25 were included in the *graph*. The complete list that contains the results of GSEA analysis is provided in Supplementary Tables 8–9. GSEA enrichment plots of WP_pancreatic_adenocarcinoma_pathway (M39732) positively correlated in (*H*) KC cells and negatively correlated in (*I*) PC cells and (*J*) KPC cells compared to control.

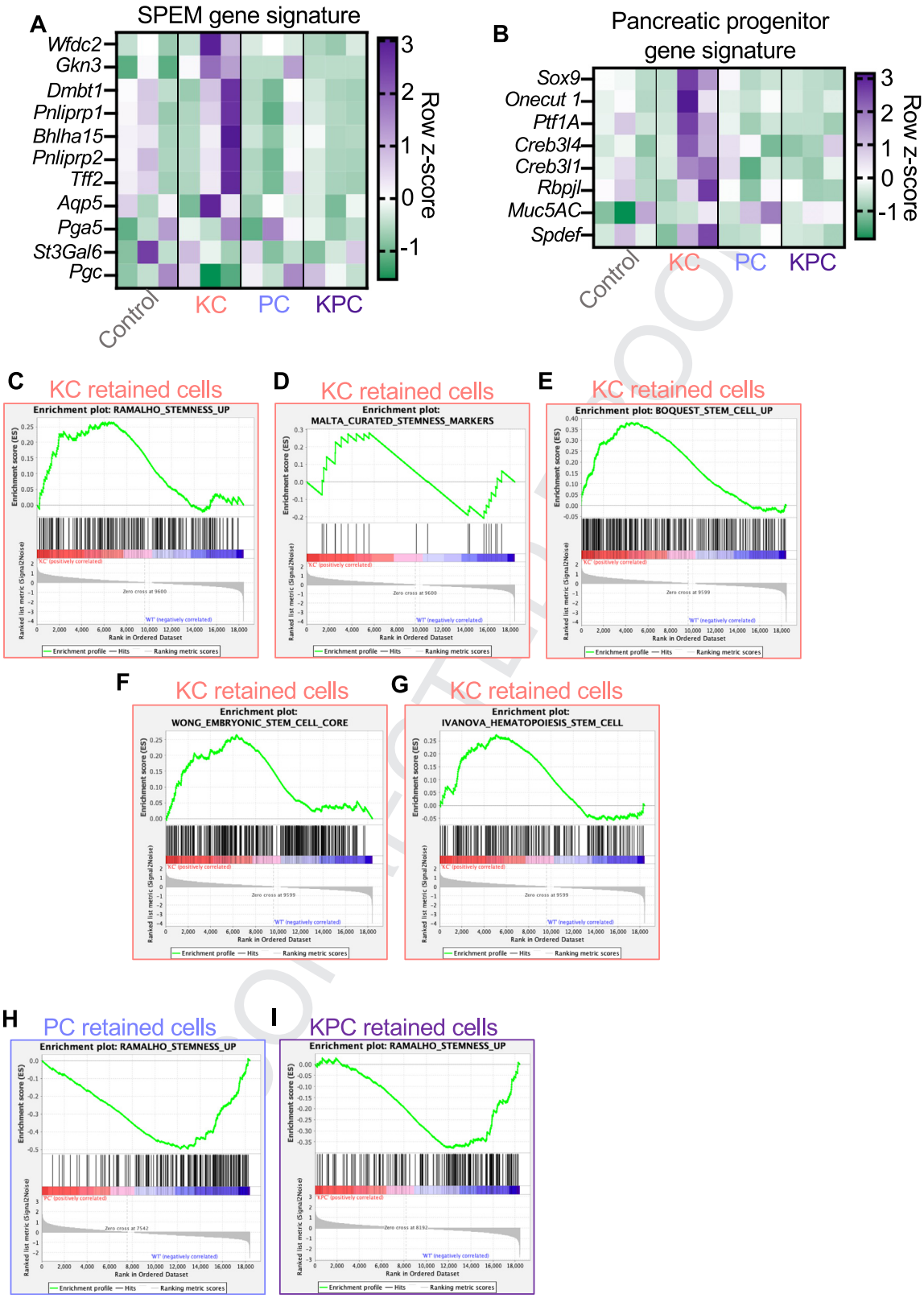

print & web 4C/FPO

Supplementary Figure 3. Noneliminated KrasG12D (KC) are stem-like, whereas p53R172H-expressing populations are not. (*A, B*) *Heatmaps* showing gene expression in noneliminated KrasG12D (KC) cells and control of (*A*) spasmolytic polypeptide-expressing metaplasia and (*B*) pancreatic lineage. *Heatmaps* show row *z* scores for the expression of each gene for 3 samples (3 pooled mice per sample) per genotype obtained from the RNA sequencing experiment. Genes are listed in *rows*, genotypes in *columns*. GSEA enrichment plots indicate positive correlation in KC retained cells compared to control for (*C*) Enrichment of Ramalho_stemness_up (M9473), (*D*) Malta_curated_stemness_markers (M30411) (embryonic, neural, and hematopoietic stem cells), (*E*) Boquest_stem_cell_up (M1834), (*F*) Wong_embryonic_stem_cell_core (M7079), and (*G*) Ivannova_hematopoiesis_-stem_cell (M6813). GSEA enrichment plots indicate negative correlation for Ramalho_Stemness_up (M30411) in (*H*) p53R172H (PC) retained cells and (A) KrasG12D p53R172H (KPC) retained cells compared to control. For more information on source data see Supplementary Table 13.

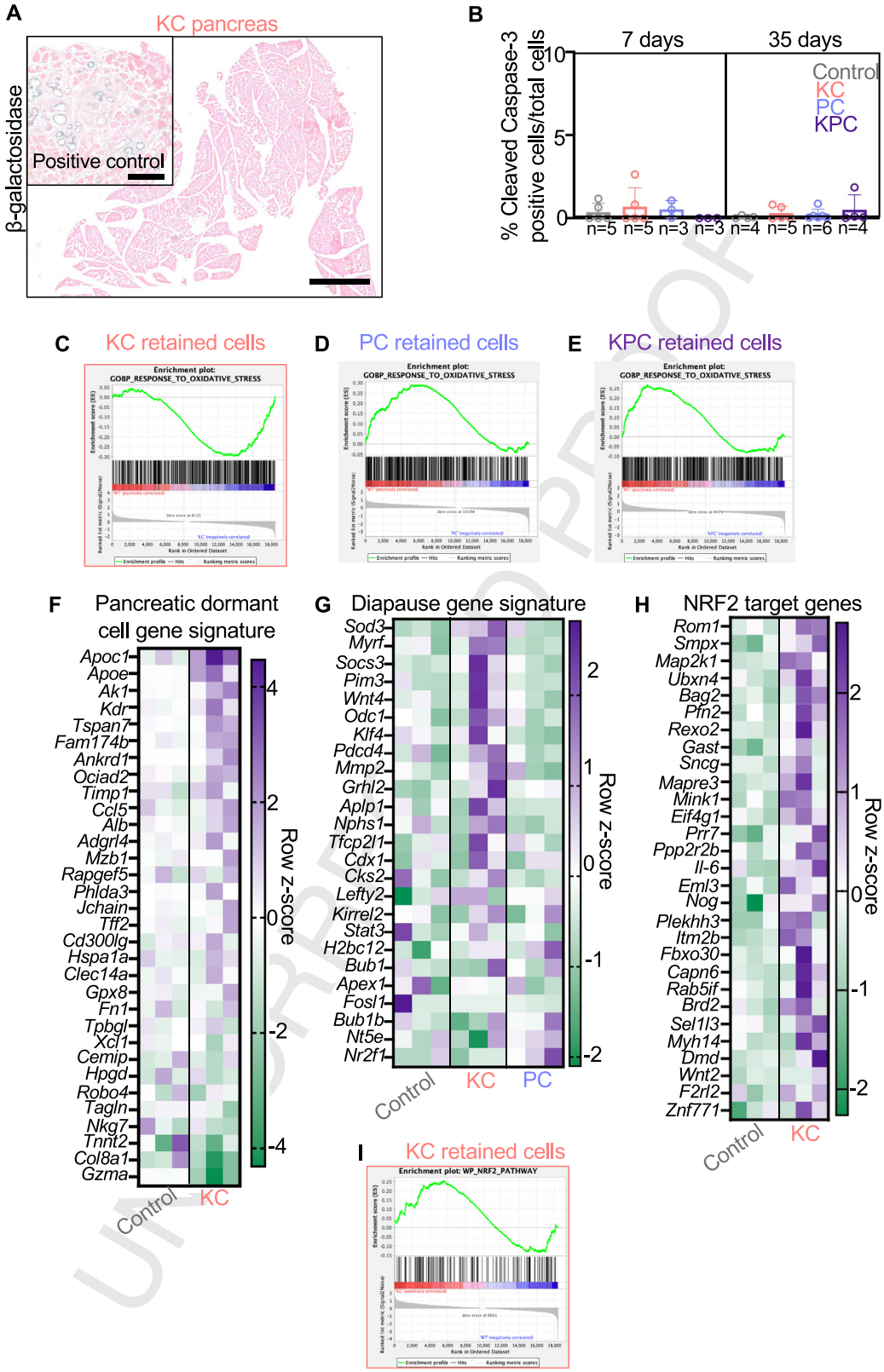

Supplementary Figure 4. Noneliminated KrasG12D cells up-regulate cell dormancy-associated pathways. (*A*) Representative *images* of β-galactosidase staining of pancreas tissue harvested from a KrasG12D (KC) mouse at 35 days p.i. (*scale bar:* 1000 μm) and in PanIN lesions as positive control (*scale bar:* 250 μm). (*B*) Percentage of cleaved caspase-3–positive cells/total cells in control, KC, p53R172H (PC) or double-mutant (KPC) pancreas tissues harvested at 7 and 35 days p.i. mean $\pm$ SD per mouse. N $=$ number of mice described in the *graph*. (*C, D, E*) GSEA enrichment plots for GOBP_RESPONSE_TO_OXIDATIVE_STRESS (M3223) showing (*C*) negative correlation in KC retained cell signatures compared to control; positive correlation for (*D*) PC and (*E*) KPC retained cell signatures compared to control. *Heatmaps* showing gene expression in (*F*) pancreatic dormant cell gene signature[e2] (*G*) diapause gene expression[22] and (*H*) NRF2 target genes (NRF2_Q4 M14141) (*rows*) in control, KC or p53R172H (PC) cell transcriptomes (columns). The *heatmap* shows row *z* scores for each gene obtained from 3 samples per genotype (3 pooled mice per samples) from the RNA sequencing experiment. Only genes with *z* scores of a fold change of 2 (*F*) or 2.25 (*H*) are shown. The full list of genes can be found in Supplementary Tables 12 and 13. (*I*) GSEA enrichment plots showing positive correlation in KC retained cells compared to control for WP_NRF2_pathway (M39454).

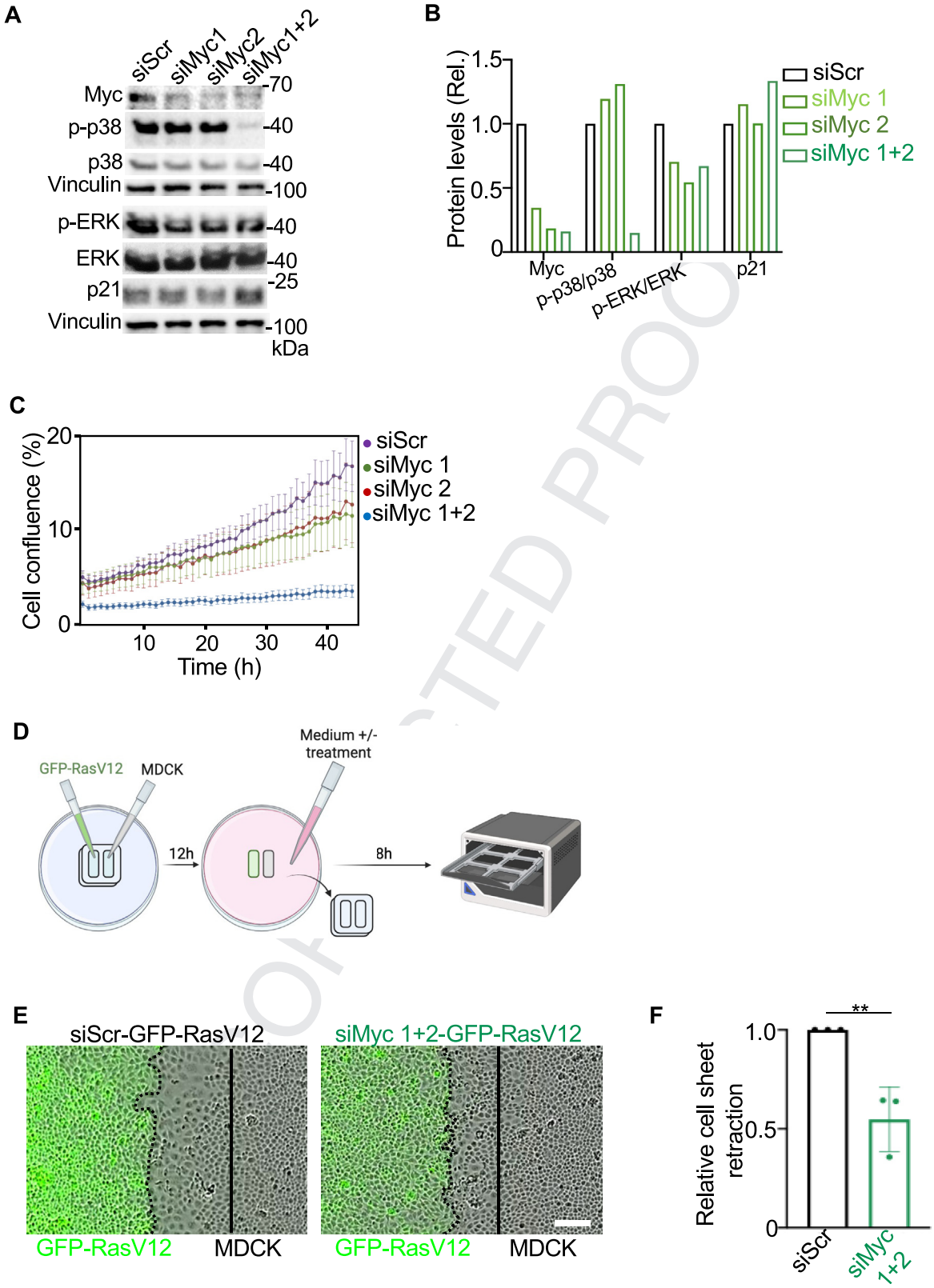

Supplementary Figure 5. Cell cycle arrest abrogates RasV12 cell extrusion in vitro. (*A*) Immunodetection of indicated antigens in GFP-RasV12 cells transfected with scrambled siRNA (siScr) or 2 siRNA oligos targeting endogenous *Myc* (siMyc1, siMyc2 or combined siMyc1+2). Lysates were collected 48 hours after transfection. p-p38, phospho-p38; p-ERK, phospho-ERK. Anti-vinculin staining was included as protein loading control. (*B*) Quantification of protein levels in the blot in (*A*). Values are relative to siScr protein levels. (*C*) Real-time cell confluence of GFP-RasV12 cells transfected with different siRNAs as quantified via Incucyte S3 imaging. Cell confluence was determined in cells 12 hours post siRNA transfection over 48 hours. Data indicate mean ± SD for 3 experiments per condition. (*D*) Schematic representation of cell confrontation assay experiments. Illustration created with BioRender.com. (*E*) Representative time-lapse images of cell confrontation assays. GFP-RasV12 cells expressing either siScr or siMyc1+2 confront nonlabeled parental MDCK cells. *Dashed lines* highlight the border between GFP-RasV12 cells and MDCK cells. *Solid lines* indicate MDCK cell migration front at the beginning of the experiment. *Scale bar:* 100 μm. (*F*) Relative retraction distance during 24 hours of siScr-GFP-RasV12 (*black bar*) or combined Myc1+2 siRNA (*green bar*) after collision with parental MDCK. Results are presented as retraction distance in siMyc-GFP-RasV12 relative to siScr-GFP-RasV12. Data represent mean ± SD measurements of 3 experiments. Student *t* test was used to analyze the data. $^{**}P < .005$.

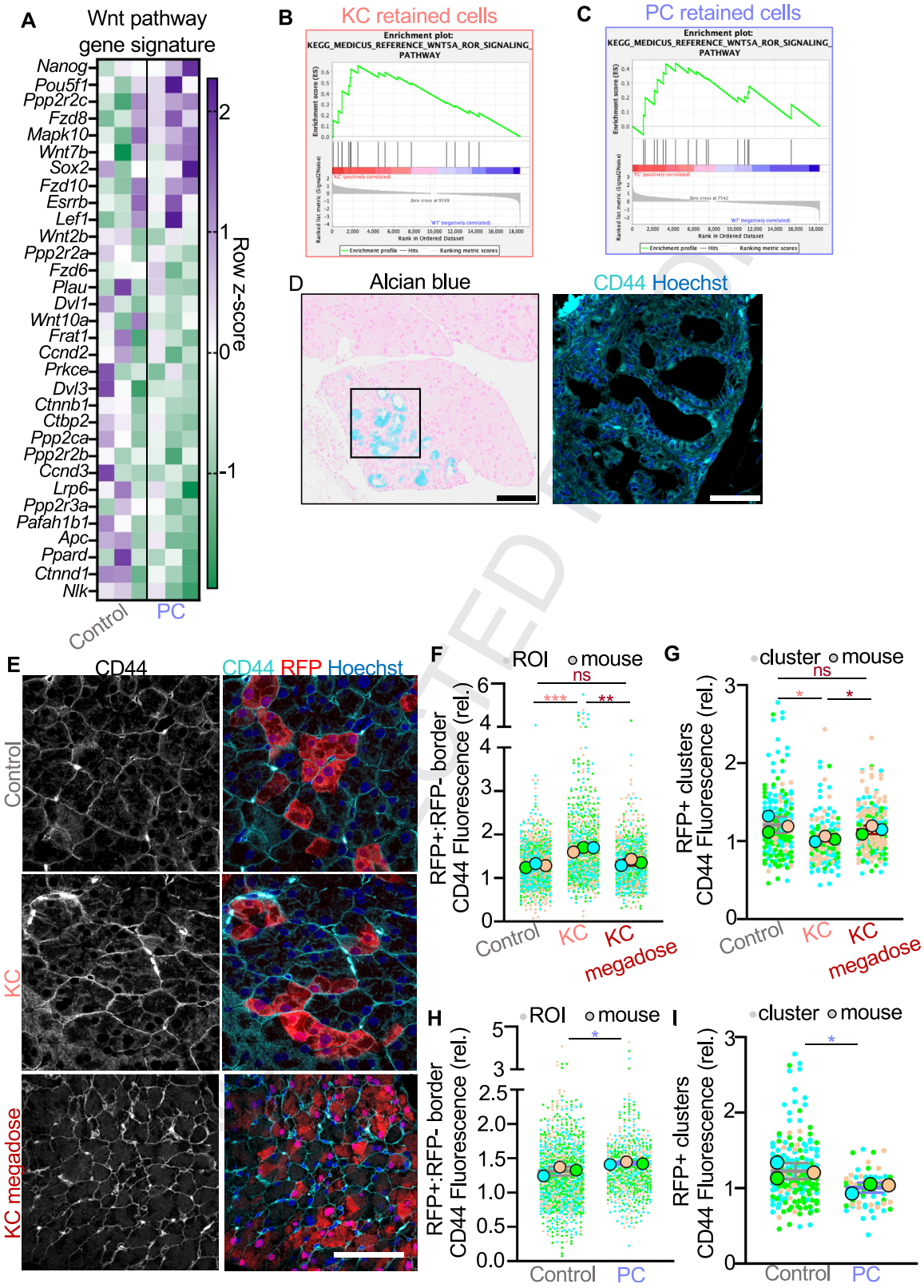

print & web 4C/FPO

Supplementary Figure 6. Wnt pathway is active in noneliminated KrasG12D or p53R172H cells. (*A*) *Heatmap* of Wnt signaling pathway (WP_Wnt_signaling, MM15829) related genes (rows) in Control and p53R712H (PC) cell transcriptomes (*columns*). The *heatmap* shows row *z* scores for each gene obtained from the RNA sequencing experiment. Only genes with *z* scores of a fold-change of 2 are shown in the Wnt pathway panel. The full list of genes can be found in Supplementary Table 11. GSEA enrichment analysis plots showing positive correlation in (*B*) KrasG12D (KC) and (*C*) PC retained cells compared with control for the KEGG_MEDICUS_reference_WNT5A_ROR_signaling_pathway (M47822). (*D*) Representative *images* of PanINs in pancreas tissue sections harvested from KC mice at 140 days p.i. *Left:* Mucin-positive PanINs (*blue*). *Scale bar:* 100 μm. *Right:* Confocal image of anti-CD44 antibody (*cyan*) labeling and Hoechst (*blue*) in PanINs in a consecutive tissue slice. *Scale bar:* 50 μm. (*E*) Representative confocal *images* of pancreas tissues harvested at 35 days p.i. stained with CD44 and RFP from Control, KC and KrasG12D high-dose tamoxifen (9 mg/40 g over 5 days, KC megadose) mice. *Scale bar:* 50 μm. (*F–I*) Mean fluorescence intensity relative to background of CD44 at the boundary between RFP-positive and RFP-negative cells (*F, H*) or in entire RFP-positive clusters (*G, I*) in control, KrasG12D low-dose (1 mg/40 g, KC) and KrasG12D high-dose tamoxifen (KC megadose) tissues (*F, G*) or control and PC tissues (*H, I*) harvested at 35 days p.i. CD44 fluorescence was quantified and reported as in Figure 4*H*. *SuperPlot* shows all the quantified regions of interest (ROI) (*F, H*) or RFP-positive clusters (*G, I*) (*smaller circles*) and the mean for each mouse (n = 3 samples; *larger circles*). The graphs show mean ± SD for the 3 mice. $^{*}P < .05$; $^{**}P < .001$; $^{***}P < .0001$. ns, $P > .05$ (Student *t* test).

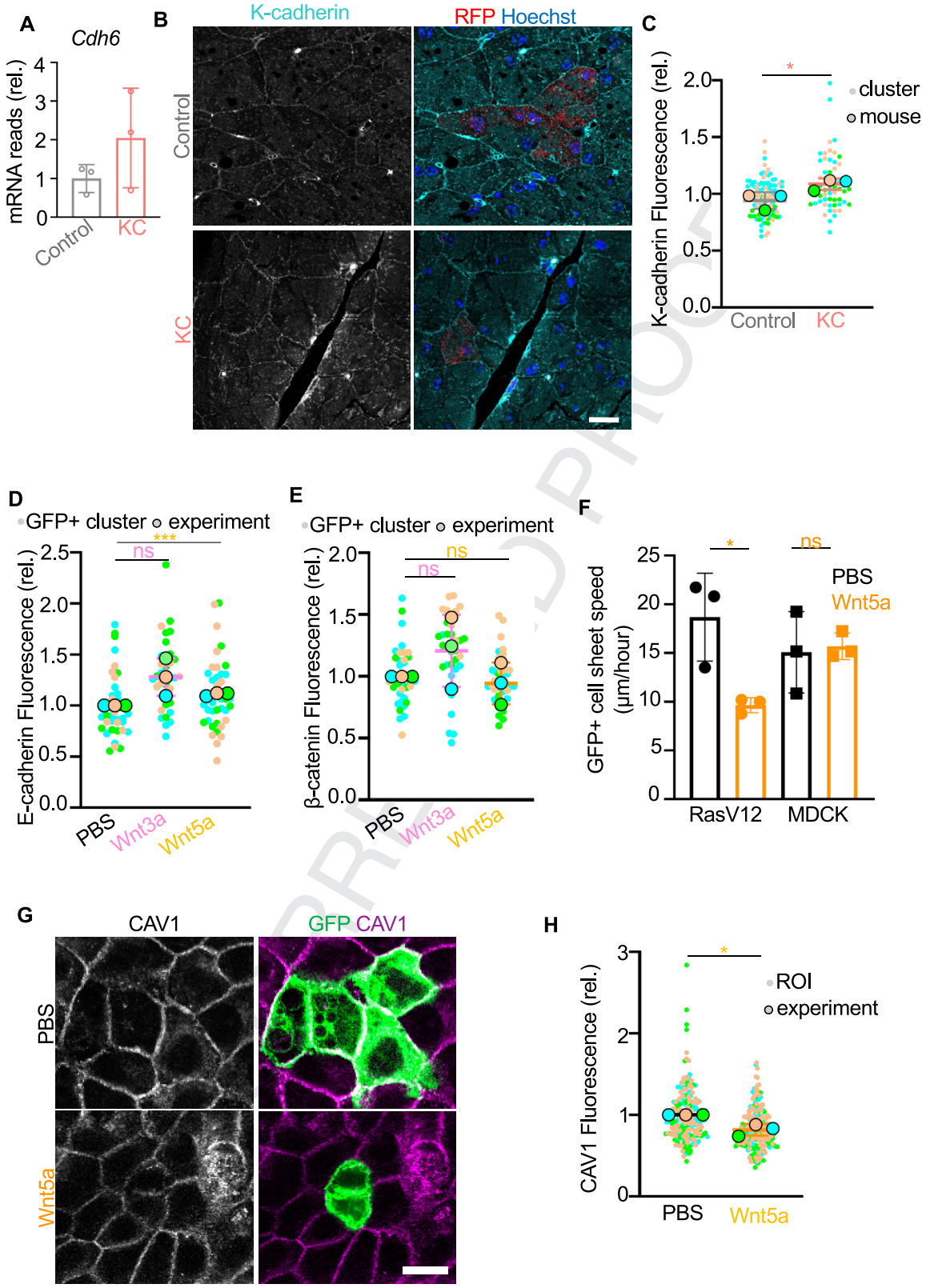

Supplementary Figure 7. Wnt5a increases RasV12 cell cohesion. (*A*) *Cdh6* messenger RNA reads relative to control reads in the 3 samples in control and 3 samples in KrasG12D (KC) obtained from the RNA sequencing experiment. *Graph* represents mean ± SD reads. (*B*) Representative confocal *images* of pancreas tissues stained with K-cadherin and RFP harvested at 35 days p.i. from control and KC mice. *Scale bar:* 50 μm. (*C*) Mean fluorescence intensity relative to background of K-cadherin RFP-positive clusters in control or KC pancreas tissues harvested at 35 days p.i. *SuperPlot* shows all the quantified RFP^+ clusters (*smaller circles*) and the mean for each mouse (n = 3 samples; *larger circles*). The *graph* shows mean ± SD for the 3 mice. $^*P = .0474$ (Student *t* test). (*D, E, H*) Mean fluorescence intensity of E-cadherin (*D*), β-catenin (*E*), or Caveolin-1 (CAV1) (*H*) in GFP-RasV12 cell clusters (mixed with MDCK cells) treated with PBS (*black*), Wnt3a (*pink*), or Wnt5a (*yellow*) for 30 hours (*D, E*) or 16 hours (*H*) relative to PBS-treated cells. *SuperPlot* shows all the quantified GFP-RasV12 clusters (*smaller circles*) and the mean for each experiment (n = 3 samples; *larger circles*). The *graphs* show mean ± SD for the 3 experiments. $^*P = .0117$; $^{***}P = .0003$; ns, $P > .05$ (Student *t* test). (*F*) Cell speed (μm/h) at which RasV12 (*circles*) or MDCK (*squares*) cells treated with PBS (*black*) or Wnt5a (*yellow*) migrate. The data represent mean ± SD from 3 independent experiment. $^*P = .0268$; ns, $P = .8202$ (Student *t* test). (*G*) Confocal *images* of CAV1 in GFP-RasV12 cells mixed with MDCK cells treated with PBS or Wnt5a for 16 hours. *Scale bar:* 20 μm.

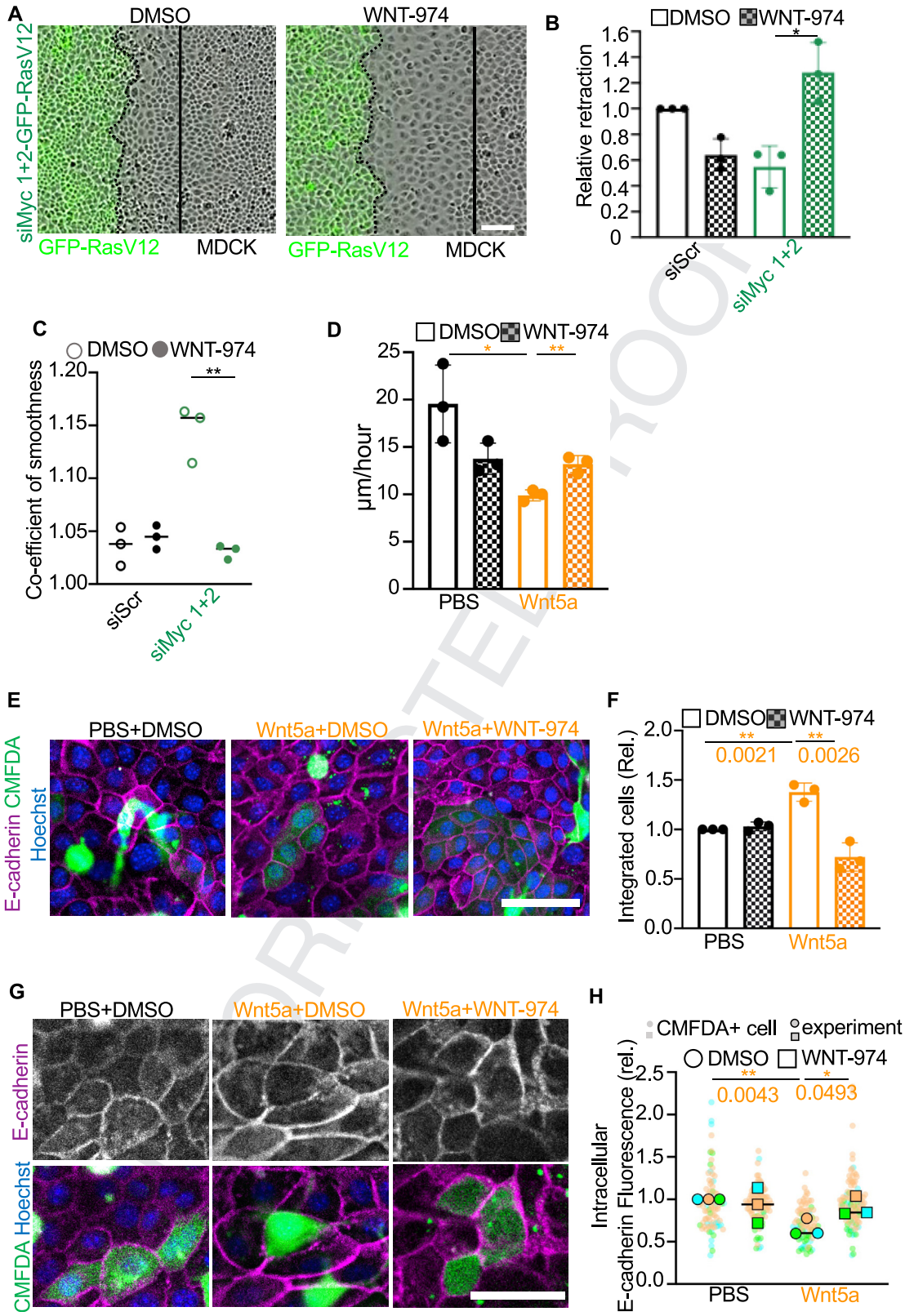

Supplementary Figure 8. Cell cycle arrest and Wnt signaling prevent GFP-RasV12/KC-TDEC segregation from normal MDCK/PDEC cells in vitro. (*A*) Representative time-lapse images of cell confrontation assays. GFP-RasV12 cells expressing combined Myc1+2 siRNA (siMyc 1+2-GFP-RasV12) confront nonlabeled parental MDCK cells. Assays were conducted in the presence of DMSO or WNT-974 (1 mM). *Dashed lines* highlight the border between GFP-RasV12 cells and MDCK cells. *Solid lines* indicate migration front of MDCK cells at the beginning of the experiment. *Scale bar:* 100 μm. (*B*) Retraction distance of GFP-RasV12 cells transfected with siScr; *black bars*) or siMyc-GFP-RasV12; *green bars*) after collision with parental MDCK cells until 24 hours later. Assays were conducted in the presence of DMSO (*solid bars*) or WNT-974 (*hatched bars*). Values are relative to PBS-/DMSO-treated cells. Data represent mean ± SD of 3 experiments. $^{*}P < .05$ (Student *t* test). (*C*) Coefficient of boundary smoothness in cell confrontation assay. Data represent mean ± SD of 3 experiments. $^{**}P < .005$ (Student *t* test). (*C*) Cell speed (μm/h) at which RasV12 cells treated with PBS (*black*) or Wnt5a (*yellow*) and DMSO or WNT-974 migrate. The data represent mean ± SD from 3 independent experiment. $^{*}P = .0156$; $^{**}P = .0058$ (Student *t* test). (*E, G)* Confocal *images* of transformed KrasG12D ductal epithelial cells (*green*) mixed with nontransformed PDECs at 1:50 ratios in vitro showing integrated/nonintegrated KrasG12D cells (*E*) or E-cadherin intracellular levels (*G*). Cells were pretreated with PBS (*black*) or Wnt5a (*orange*) for 6 hours and fixed 48 hours after mixing and DMSO or WNT-974 treatment. *Scale bar:* 50 μm. (*F*) Proportion of integrated KrasG12D ductal epithelial cells relative to integrated PBS-/DMSO-treated KrasG12D ductal epithelial cells (n = 3 experiments). Cells were treated as in E. Data represent mean ± SD. Student *t* test was used to analyze the data. $^{**}P < .001$. (*H*) Mean fluorescence intensity of intracellular E-cadherin in KrasG12D ductal epithelial cells relative to PBS-/DMSO-treated cells (n = 3 experiments). Cells were treated as in (*E*). Data represent mean ± SD. Student *t* test was used to analyze the data. $^{*}P < .05$; $^{**}P < .001$.

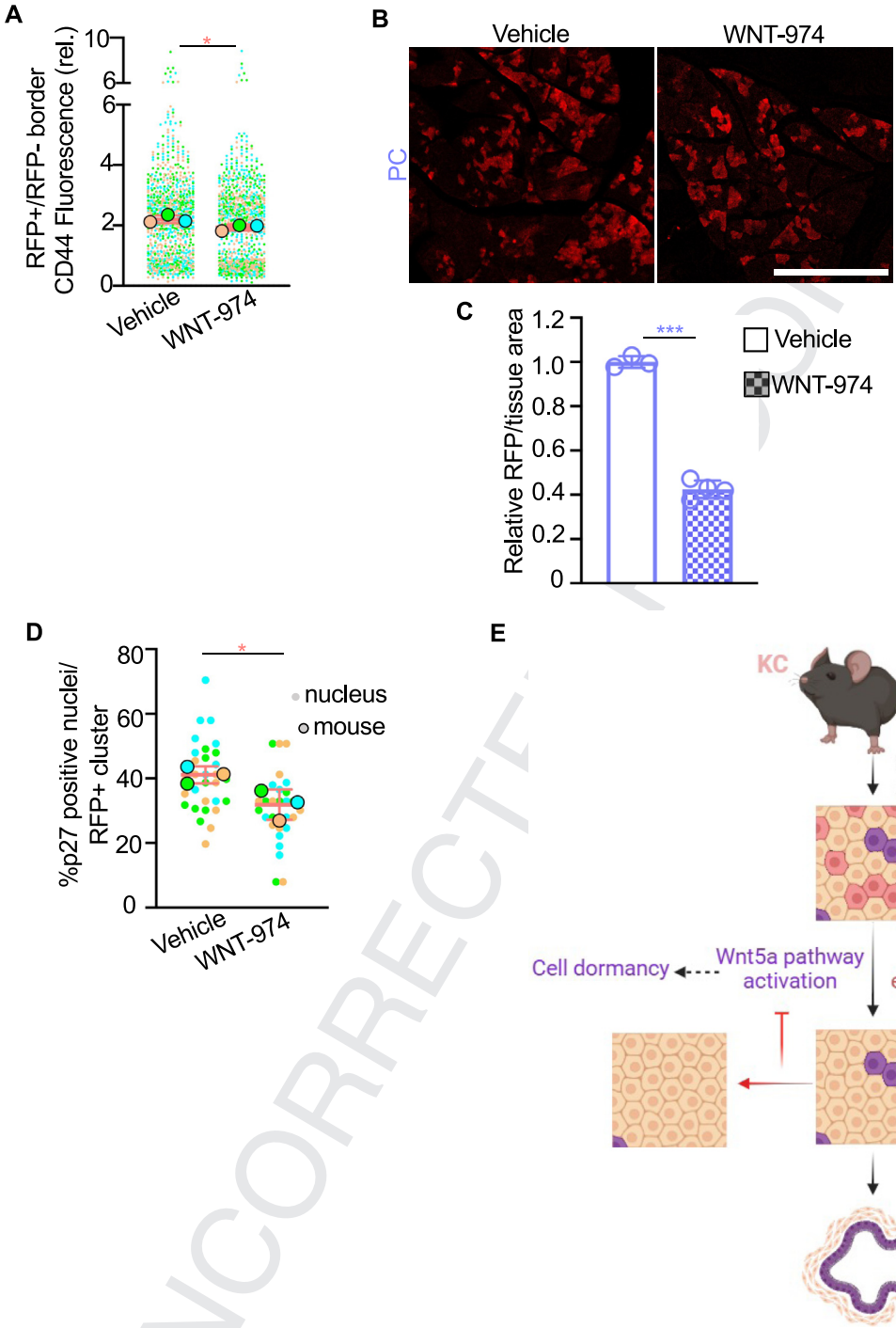

Supplementary Figure 9. Wnt signaling inhibition promotes KrasG12D (KC) cell elimination in vivo. (*A*) Mean fluorescence intensity relative to background of CD44 at the boundary between RFP-positive and RFP-negative cells in vehicle or WNT-974–treated KrasG12D (1.5 mg/kg, KC) tissues harvested at the end of the treatment (see Figure 6*H*). CD44 fluorescence was quantified and reported as in Figure 4*H*. Control quantification is the same used in Supplementary Figure 6*F*. *SuperPlot* shows all the quantified regions of interest (ROIs) (*smaller circles*) and the mean for each mouse (n = 3 samples; *larger circles*). The *graph* shows mean ± SD for the 3 mice. Student *t* test was used to analyze the data. $^{*}P = .0467$. (*B*) Representative *images* of endogenous RFP fluorescence in PC pancreas tissue sections harvested 28 days post treatment with vehicle or WNT-974 (1.5 mg/kg). *Scale bar:* 500 μm. (*C*) Percentage of RFP area in PC mice treated with WNT-974 or vehicle and relative to vehicle-treated tissues. Data represent mean ± SD per mouse. Student *t* test was used to analyze the data, $^{***}P < .0005$. (*D*) Percentage of p27-positive nuclei in RFP^{+} clusters from KC tissues treated with vehicle or WNT-974. Data represent mean ± SD per mouse. Student *t* test was used to analyze the data, $^{*}P = .0410$. (*E*) Schematic summarizing the main findings of the study. Illustration created with BioRender.com.

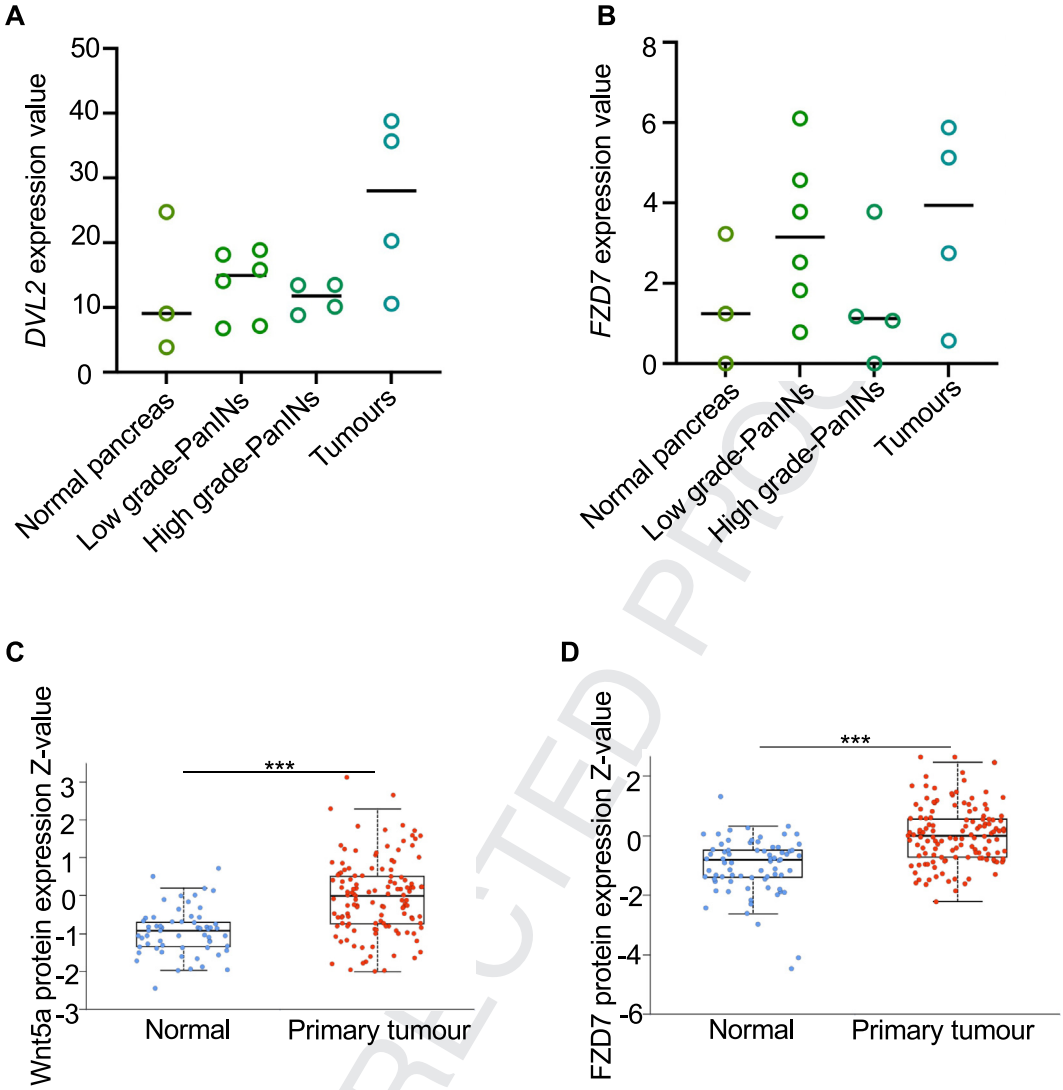

Supplementary Figure 10. Components of the WNT5A-ROR signaling pathway are up-regulated in human pancreatic cancer. *DVL2* (*A*) and *FZD7* (*B*) expression levels in normal pancreas, low-grade PanINs, high-grade PanINs, and tumors (GSE210351). (*C, D*) The *z* value of Wnt5a (*C*) or FZD7 (*D*) protein in normal pancreas (*blue*) and pancreatic adenocarcinoma (*red*). The *box plots* show individual values for each sample; normal n = 74; primary tumor n = 137. Student *t* tests were used to analyze the data. *$P = .032$; ***$P < .0001$. The data were obtained from the Clinical Proteomic Tumour Analysis Consortium.

Supplementary Table 14.XXXX Q23

Antibody and fluorescence stains	Application	Antigen Retrieval	Dilution	Source	Identifier
Ki-67	IHC, IF	ProK 15’	1:500	Abcam	ab16667
CC-3	IHC	Citrate pH 6 15’	1:300	Cell Signaling	9661s
RFP	IHC, IF	ProK 15’	1:500	Rockland	600-401-379
Lectin PNA-A488	FACS	—		Invitrogen	L21409
c-Myc	WB	—	1:500	Santa Cruz	sc788
Phospho-p38	WB	—	1:1000	Cell Signaling	9211s
p38a	WB	—	1:1000	Santa Cruz	sc136210
Vinculin	WB	—	1:1000	Sigma Aldrich	V4505
Phospho-ERK	WB	—	1:1000	—	—
ERK	WB	—	1:1000	Cell Signaling	—
p21WAP/Cip	WB	—	1:1000	Sigma Aldrich	P1484
CD44	IF	ProK 15’	1:25	Cell Signaling	3570S
K-cadherin	IF	PoK 15’	1:50	ThermoFisher	MA1-06305
β-catenin	IF	Citrate pH 6 15’	1:50	BD Biosciences	610154
RFP	IF	Citrate pH 6 15’	1:500	Creative Diagnosis	DPATB-H83194
E-cadherin	IF	Citrate pH 6 15’	1:1000	BD Biosciences	610182
p27	IF	—	1:25	Santa Cruz	SC-528
Sox9	IF	—	1:100	ThermoFisher	PA5-81966
Wnt5a	IF	—	1:50	Santa Cruz	SC-30224
Dvl2	IF	—		Santa Cruz	SC-13974
goat anti-rabbit AF568	IF	—	1:1000	ThermoFisher	A-11011
donkey anti-mouse AF488		—	1:1000	ThermoFisher	A-21202
goat anti-rabbit AF488	IF	—	1:1000	ThermoFisher	A-11008
goat anti-rabbit HRP	WB	—	1:5000	Vector Laboratories	MP-7451-15
goat anti-mouse HRP	WB	—	1:5000	Vector Laboratories	MP-7802-15
Phalloidin	IF	—	1:1000	Sigma Aldrich	65906
E-cadherin	IF	—	1:100	ThermoFisher	13-1900
Caveolin	IF	—	1:50	Abcam	Ad2910
Hoechst	—	—	1:1000	ThermoFisher	H3570

FACS, fluorescence-activated cell sorted; IF, immunofluorescence; IHC, immunohistochemistry; WB, western blot.